

FEATURE-ALIGNED N-BEATS WITH SINKHORN DIVERGENCE

Joonhun Lee^{*1}, Myeongho Jeon^{*1}, Myungjoo Kang^{†1}, Kyunghyun Park^{†2}
 Seoul National University¹, Nanyang Technological University²
 {niceguy718, andyjeon, mkang}@snu.ac.kr, kyunghyun.park@ntu.edu.sg

ABSTRACT

We propose Feature-aligned N-BEATS as a domain-generalized time series forecasting model. It is a nontrivial extension of N-BEATS with doubly residual stacking principle (Oreshkin et al. [42]) into a representation learning framework. In particular, it revolves around marginal feature probability measures induced by the intricate composition of residual and feature extracting operators of N-BEATS in each stack and aligns them stack-wisely via an approximate of an optimal transport distance referred to as the Sinkhorn divergence. The training loss consists of an empirical risk minimization from multiple source domains, i.e., forecasting loss, and an alignment loss calculated with the Sinkhorn divergence, which allows the model to learn invariant features stack-wisely across multiple source data sequences while retaining N-BEATS’s interpretable design and forecasting power. Comprehensive experimental evaluations with ablation studies are provided and the corresponding results demonstrate the proposed model’s forecasting and generalization capabilities.

1 INTRODUCTION

Machine learning models typically presume that the loss minimization from training data results in reasonable performance on a target environment, i.e., empirical risk minimization [53]. However, when using such models in the real world, the target environment is likely to deviate from the training data, which poses a significant challenge for a well-adaptive model to the target environment. This is related to the concept of *domain shift* [46].

A substantial body of research has been dedicated to developing frameworks that can accommodate the domain shift issue [5, 6, 19]. In particular, classification tasks have been the predominant focus [29, 31, 55, 56, 63]. As an integral way for modeling sequential data in broad domains such as finance, operation research, climate modeling, and biostatistics, *time series forecasting* has been a big part of machine learning fields. Nevertheless, the potential domain shift issue for common forecasting tasks has not been considered intensively compared to classification tasks, but only a few articles addressing this can be named [24, 25].

The goal of this article is to propose a resolution for the domain shift issue within time series forecasting tasks, namely a *domain-generalized* time-series forecasting model. In particular, the proposed model is built upon a purely deep learning-based model which is N-BEATS proposed by [42, 43], and a representation learning toolkit which is the *feature alignment*. N-BEATS revolves around a doubly residual stacking principle and enhances the forecasting capabilities of multilayer perceptron (MLP) architectures without resorting to any traditional machine learning methods. On the other hand, it is well-known that aligning marginal feature measures enables machine learning models to capture invariant features across distinctive domains [7]. Indeed, in the context of classification tasks, many references [29, 35, 39, 62] demonstrated that the feature alignment mitigates the domain shift issue.

It is important to highlight that the model is not a straightforward combination of the established components but a nontrivial extension that poses several challenges. First, N-BEATS does not allow the feature alignment in a ‘one-shot’ unlike the aforementioned references. This is because it is a

^{*}Equal contribution [†]Co-corresponding authors

hierarchical multi-stacking architecture in which each stack consists of several blocks and is connected to each other by residual operations and feature extractions. In response to this, we devise the *stack-wise* alignment that is a minimization of divergences between marginal feature measures on a stack-wise basis. The stack-wise alignment enables the model to learn feature invariance with an ideal frequency of propagation. Indeed, instead of aligning every block for each stack, single alignment for each stack mitigates gradient vanishing/exploding issue [44] via sparsely propagating loss while preserving N-BEATS’ the interpretability and ample semantic coverage [42, Section 3.3].

Second, the stack-wise alignment demands an efficient and accurate method for measuring divergence between measures. Indeed, the alignment is inspired by the error analysis of general domain generalization models given in [1, Theorem 1], in which empirical risk minimization loss and pairwise \mathcal{H} -divergence loss between marginal feature measures are the trainable components among the total error terms without any target domain information. In particular, since the feature alignment requires the calculation of pairwise divergences for multiple stacks (due to the doubly residual stacking principle), the computational load steeply increases as either the number of source domains or that of stacks increases. On the other hand, from the perspective of accuracy and efficiency, the \mathcal{H} -divergence is notoriously challenging to be used in practice [5, 27, 30, 51].

For a suitable toolkit, we adopt the Sinkhorn divergence which is an efficient approximation for the classic optimal transport distances [16, 20, 47]. This choice is motivated by the substantial theoretical evidences of optimal transport distances. Indeed, in the adversarial framework, optimal transport distances have been essential for theoretical evidences and calculation of divergences between push-forward measures induced by a generator and a target measure [20, 50, 59, 63]. In particular, the computational efficiency of the Sinkhorn divergence and fluent theoretical results by [12, 13, 16, 20] are crucial for our choice among other optimal transport distances. Thereby, the training objective is to minimize the empirical risk and the stack-wise Sinkhorn divergences (Section 3.3).

Contributions. To provide an informative procedure of stack-wise feature alignment, we introduce a concrete mathematical formulation of N-BEATS (Section 2.2), which enables to define the push-forward feature measures induced by the intricate residual operations and the feature extractions for each stack (Section 3.1). From this, we make use of theoretical properties of optimal transport problems to show a representation learning bound for the stack-wise feature alignment with the Sinkhorn divergence (Theorem 3.6), which justifies the feasibility of Feature-aligned N-BEATS. To embrace comprehensive domain generalization scenarios, we use real-world data and evaluate the proposed method under three distinct protocols based on the domain shift degree. We show that the model consistently outperforms other forecasting models. In particular, our method exhibits outstanding generalization capabilities under severe domain shift cases (Table 1). We further conduct ablation studies to support the choice of the Sinkhorn divergence in our model (Table 2).

Related literature. For time-series forecasting, deep learning architectures including recurrent neural networks [3, 8, 23, 48, 49] and convolutional neural networks [10, 33] have achieved significant progress. Recently, a prominent shift has been observed towards transformer architectures leveraging self-attention mechanisms [32, 34, 57, 58, 64, 65]. Despite their innovations, concerns have been raised regarding the inherent permutation invariance in self-attention, which potentially leads to the loss of temporal information [60]. On the other hand, [9, 42] empirically show that MLP-based architectures would mitigate such a disadvantage and even surpass the transformer-based models.

Regarding the domain shifts for time series modeling, [24] proposed a technique that selects samples from source domains resembling the target domain, and employs regularization to encourage learning domain invariance. [25] designed a shared attention module paired with a domain discriminator to capture domain invariance. [43] explored domain generalization from a meta-learning perspective without the information on the target domain. Nonetheless, an explicit toolkit and concrete formulation for domain generalization is not considered therein.

2 BACKGROUND

Notations. Let $\mathcal{X} := \mathbb{R}^\alpha$ and $\mathcal{Y} := \mathbb{R}^\beta$ be the input and output spaces, respectively, where α and β denote the lookback and forecast horizons, respectively. Let $\mathcal{Z} := \mathbb{R}^\gamma$ be the latent space with γ representing the feature dimension. We further denote by $\tilde{\mathcal{Z}} \subset \mathcal{Z}$ a subspace of \mathcal{Z} . All the aforementioned spaces are equipped with the Euclidean norm $\|\cdot\|$. Define by $\mathcal{P} := \mathcal{P}(\mathcal{X} \times \mathcal{Y})$

the set of all Borel joint probability measures on $\mathcal{X} \times \mathcal{Y}$. For any $\mathbb{P} \in \mathcal{P}$, denotes by $\mathbb{P}_{\mathcal{X}}$ and $\mathbb{P}_{\mathcal{Y}}$ corresponding marginal probability measures on \mathcal{X} and \mathcal{Y} , respectively. We further define by $\mathcal{P}(\mathcal{X})$ and $\mathcal{P}(\tilde{\mathcal{Z}})$ the sets of all Borel probability measures on \mathcal{X} and $\tilde{\mathcal{Z}}$, respectively.

2.1 DOMAIN GENERALIZATION IN TIME SERIES FORECASTING

There are multiple source domains $\{\mathcal{D}^k\}_{k=1}^K$ with $K \geq 2$ and target (unseen) domain \mathcal{D}^T . Assume that each \mathcal{D}^k is equipped with $\mathbb{P}^k \in \mathcal{P}$ and the same holds for \mathcal{D}^T with $\mathbb{P}^T \in \mathcal{P}$ and that sequential data for each domain are sampled from corresponding joint distribution. Let $l : \mathcal{Y} \times \mathcal{Y} \rightarrow \mathbb{R}_+$ be a loss function. Then, the objective is to derive a prediction model $\mathfrak{F} : \mathcal{X} \rightarrow \mathcal{Y}$ such that $\mathfrak{F}(\mathbf{s}_{t-\alpha+1}, \dots, \mathbf{s}_t) \approx \mathbf{s}_{t+1}, \dots, \mathbf{s}_{t+\beta}$ for $\mathbf{s} = (\mathbf{s}_{t-\alpha+1}, \dots, \mathbf{s}_t) \times (\mathbf{s}_{t+1}, \dots, \mathbf{s}_{t+\beta}) \sim \mathbb{P}^T$, by leveraging on $\{\mathbb{P}^k\}_{k=1}^K$, i.e.,

$$\inf_{\mathfrak{F}} \mathcal{L}(\mathfrak{F}), \quad \text{with} \quad \mathcal{L}(\mathfrak{F}) := \frac{1}{K} \sum_{k=1}^K \mathbb{E}_{(x,y) \sim \mathbb{P}^k} [l(\mathfrak{F}(x), y)]. \quad (2.1)$$

2.2 DOUBLY RESIDUAL STACKING ARCHITECTURE

The main architecture of N-BEATS equipped with the doubly residual stacking principle from [9, 42] is summarized as follows: for $M, L \in \mathbb{N}$, the model comprises M stacks, with each stack consisting of L blocks. The blocks share the same model weight within each respective stack and are recurrently operated based on the double residual stacking principle. More precisely, an m -th stack derives the principle in a way that for $x_{m,1} \in \mathcal{X}$,

$$\hat{y}_m := \sum_{l=1}^L (\xi_{\downarrow}^m \circ \psi^m)(x_{m,l}), \quad x_{m,l} := x_{m,l-1} - (\xi_{\uparrow}^m \circ \psi^m)(x_{m,l-1}), \quad l = 2, \dots, L, \quad (2.2)$$

where $\psi^m : \mathcal{X} \rightarrow \mathcal{Z}$ extracts features $\psi^m(x_{m,l}) \in \mathcal{Z}$ from the inputs $x_{m,l} \in \mathcal{X}$ for each layer l , and $(\xi_{\downarrow}^m, \xi_{\uparrow}^m) : \mathcal{Z} \rightarrow \mathcal{Y} \times \mathcal{X}$ generates both forecasts $(\xi_{\downarrow}^m \circ \psi^m)(x_{m,l}) \in \mathcal{Y}$ and backcasts $(\xi_{\uparrow}^m \circ \psi^m)(x_{m,l}) \in \mathcal{X}$ branches. Note that $\hat{y}_m \in \mathcal{Y}$ represents the m -th forecast obtained through the hierarchical aggregation of each block's forecast, and that the last backcast $x_{m,L} \in \mathcal{X}$, derived by a residual sequence from blocks, serves as an input for the next stack, except for the case $m = M$.

Once the hierarchical aggregation of all stacks and the residual operations are completed, the model \mathfrak{F} for the doubly residual stacking architecture is given as follows: for $(x, y) \sim \mathbb{P}^T$ and $x_{1,1} := x$,

$$y \approx \mathfrak{F}(x; \Psi, \Xi_{\downarrow}, \Xi_{\uparrow}) := \sum_{m=1}^M \hat{y}_m, \quad \text{and} \quad x_{m,1} := x_{m-1,L}, \quad m = 2, \dots, M, \quad (2.3)$$

subject to \hat{y}_m and $x_{m-1,L}$ given in (2.2), where

$$\Psi := \{\psi^m\}_{m=1}^M, \quad \Xi_{\downarrow} := \{\xi_{\downarrow}^m\}_{m=1}^M, \quad \text{and} \quad \Xi_{\uparrow} := \{\xi_{\uparrow}^m\}_{m=1}^M, \quad (2.4)$$

are implemented by fully connected layers. For further details, refer to Appendix A.

2.3 DOMAIN-INVARIANT FEATURE REPRESENTATION

After the investigation on the error analysis for domain adaptation models by [61], an extended version for domain generalization models is provided by [1]. This provides us an insight for developing a domain generalization toolkit within the context of doubly residual stacking models.

In the following, we restate Theorem 1 in [1]. To that end, we introduce some notations. Denote by \mathcal{H} a class of hypothesis functions $h : \mathcal{X} \rightarrow [0, 1]$ and by $d_{\mathcal{H}}(\mathbb{P}'_{\mathcal{X}}, \mathbb{P}''_{\mathcal{X}}) := 2 \sup_{h \in \mathcal{H}} |\mathbb{E}_{x \sim \mathbb{P}'_{\mathcal{X}}} [\mathbf{1}_{\{h(x)=1\}}] - \mathbb{E}_{x \sim \mathbb{P}''_{\mathcal{X}}} [\mathbf{1}_{\{h(x)=1\}}]|$ an \mathcal{H} -divergence between $\mathbb{P}'_{\mathcal{X}}, \mathbb{P}''_{\mathcal{X}} \in \mathcal{P}(\mathcal{X})$. We further denote by $\tilde{\mathcal{H}} := \{\text{sgn}(|h(\cdot) - h'(\cdot)| - t)|h, h' \in \mathcal{H}, t \in [0, 1]\}$ and by $d_{\tilde{\mathcal{H}}}(\cdot, \cdot)$ corresponding $\tilde{\mathcal{H}}$ -divergence on $\mathcal{P}(\mathcal{X})$.

Proposition 2.1. *Let Δ_K be a $(K-1)$ -dimensional simplex such that each component π represents a convex weight. Define by $\Lambda := \{\sum_{k=1}^K \pi_i \mathbb{P}_{\mathcal{X}}^k | \pi \in \Delta_K\}$ a convex hull of $\{\mathbb{P}_{\mathcal{X}}^k\}_{k=1}^K$. Denote*

by $\mathbb{P}^* := \sum_{k=1}^K \pi_k^* \mathbb{P}_{\mathcal{X}}^k \in \arg \min_{\mathbb{P}'_{\mathcal{X}} \in \Lambda} d_{\mathcal{H}}(\mathbb{P}'_{\mathcal{X}}, \mathbb{P}_{\mathcal{X}}^T)$ a minimizer. Then, an expected risk, i.e., forecasting loss, ϵ^T for target measure $\mathbb{P}_{\mathcal{X}}^T$ has an upper bound given as

$$\epsilon^T(h) \leq \sum_{k=1}^K \pi_k^* \epsilon^k(h) + d_{\mathcal{H}}(\mathbb{P}_{\mathcal{X}}^T, \mathbb{P}_{\mathcal{X}}^*) + \max_{i,j \in \{1, \dots, K\}, i \neq j} d_{\tilde{\mathcal{H}}}(\mathbb{P}_{\mathcal{X}}^i, \mathbb{P}_{\mathcal{X}}^j) + \lambda_{(\mathbb{P}_{\mathcal{X}}^T, \mathbb{P}_{\mathcal{X}}^*)}, \quad h \in \mathcal{H},$$

where $\lambda_{(\mathbb{P}_{\mathcal{X}}^T, \mathbb{P}_{\mathcal{X}}^*)} := \min\{\mathbb{E}_{x \sim \mathbb{P}_{\mathcal{X}}^T}[\|f^*(x) - f^T(x)\|], \mathbb{E}_{x \sim \mathbb{P}_{\mathcal{X}}^*}[\|f^*(x) - f^T(x)\|]\}$ with $f^* := \sum_{k=1}^K \pi_k^* f^k$, and each f^k denotes a true labeling function under \mathbb{P}^k , i.e., $y = f^k(x)$ for every $(x, y) \sim \mathbb{P}^k$, and similarly f^T denotes a true labeling function under \mathbb{P}^T .

While the upper bound consists of four terms, only the first and third terms, representing the source risks, i.e., $\{\epsilon^k\}_{k=1}^K$, and the pairwise divergences across all marginal feature measures, i.e., $\{d_{\tilde{\mathcal{H}}}(\mathbb{P}_{\mathcal{X}}^i, \mathbb{P}_{\mathcal{X}}^j)\}_{i \neq j}^K$, are learnable without the target domain information.

3 METHOD

3.1 MARGINAL FEATURE MEASURES

Aligning marginal feature measures is a predominant approach in domain-invariant representation learning [19, 52]. In particular, the marginal feature measures $\{g_{\#} \mathbb{P}_{\mathcal{X}}^k\}_{k=1}^K$ are defined as push-forward measures induced by a given feature map $g : \mathcal{X} \rightarrow \mathcal{Z}$ from $\{\mathbb{P}_{\mathcal{X}}^k\}_{k=1}^K$, i.e., $g_{\#} \mathbb{P}_{\mathcal{X}}^k(E) = \mathbb{P}_{\mathcal{X}}^k \circ g^{-1}(E)$ for any Borel set E in \mathcal{Z} .

However, defining such measures for doubly residual architectures poses some challenges. Indeed, as discussed in Section 2.2, N-BEATS includes multiple feature extractors $\Psi = \{\psi^m\}_{m=1}^M$ as defined in (2.2), where each extractor ψ^m takes a sampled input passing through multiple residual operations of previous stacks and the input is recurrently processed within each stack by the residual operations Ξ_{\downarrow} and Ξ_{\uparrow} . The scaling factor represents domain-specific characteristics that exhibit noticeable variations. This can lead to an excessive focus on scale adjustments in the aligning process, potentially neglecting crucial features, such as seasonality or trend.

To resolve these difficulties, we propose a stack-wise alignment of feature measures on subspace $\tilde{\mathcal{Z}} \subseteq \mathcal{Z}$. This involves defining measures for each stack through the compositions of feature extractions in $\Psi = \{\psi^m\}_{m=1}^M$, backcasting operators in $\Xi_{\uparrow} = \{\xi_{\uparrow}^m\}_{m=1}^M$ given in (2.2), and a normalization function.

Definition 3.1. Let $\sigma : \mathcal{Z} \rightarrow \tilde{\mathcal{Z}}$ be a normalizing function satisfying C_{σ} -Lipschitz continuity, i.e., $\|\sigma(z) - \sigma(z')\| \leq C_{\sigma} \|z - z'\|$ for $z, z' \in \mathcal{Z}$. Given $\psi^m : \mathcal{X} \rightarrow \mathcal{Z}$ defined in (2.2), the operators $r^m : \mathcal{X} \rightarrow \mathcal{X}$ and $g^m : \mathcal{X} \rightarrow \mathcal{Z}$ are defined as:

$$r^m(x) := x - (\xi_{\uparrow}^m \circ \psi^m)(x), \quad \text{and} \quad (3.1)$$

$$g^m(x) := (\psi^m \circ (r^m)^{(L-1)} \circ (r^{m-1})^{(L)} \circ \dots \circ (r^1)^{(L)})(x), \quad (3.2)$$

where $(r^m)^{(L)}$ denotes L -times composition of r^m , with $(r^m)^{(L-1)}(x) := x$ for $L - 1 = 0$ and $g^m = (\psi^m \circ (r^m)^{(L-1)})$ for $m = 1$. Then the set of marginal feature measures in the m -th stack for $m = 1, \dots, d$ is defined by

$$\{(\sigma \circ g^m)_{\#} \mathbb{P}_{\mathcal{X}}^k\}_{k=1}^K,$$

where each $(\sigma \circ g^m)_{\#} \mathbb{P}_{\mathcal{X}}^k$ is a push-forward of $\mathbb{P}_{\mathcal{X}}^k \in \{\mathbb{P}_{\mathcal{X}}^k\}_{k=1}^K$ induced by $\sigma \circ g^m : \mathcal{X} \rightarrow \tilde{\mathcal{Z}}$.

Remark 3.2. The normalization function σ helps the model to learn invariant features associated with more essential information by mitigating the influence of the scale information of each domain. Moreover, the Lipschitz condition on σ prevents gradient explosion during model updates. There are two representatives for σ :

(i) softmax : $\mathcal{Z} \rightarrow \tilde{\mathcal{Z}} = (0, 1)^{\gamma}$ with $\text{softmax}(z)_j = e^{z_j} / \sum_{i=1}^{\gamma} e^{z_i}$, $j = 1, \dots, \gamma$;

(ii) tanh: $\mathcal{Z} \rightarrow \tilde{\mathcal{Z}} = (-1, 1)^{\gamma}$ with $\text{tanh}(z)_j = (e^{2z_j} - 1) / (e^{2z_j} + 1)$, $j = 1, \dots, \gamma$.

Both are 1-Lipschitz continuous, i.e., $C_{\sigma} = 1$. In Appendix E (see Table 9), we provide the ablation study under these functions, in addition to the case without the normalization.

Remark 3.3. Embedding feature alignment ‘block-wisely’ for every stack results in recurrent operations within each stack and redundant gradient flows. This redundancy can cause exploding or vanishing gradients for long-term forecasting [44]. Our stack-wise feature alignment addresses these problems by sparsely propagating the loss. It also maintains ample alignment coverage related to semantics since the stack serves as a semantic extraction unit in [42]. Further heuristic demonstration is provided in Appendix E.1.

The operator g^m in (3.2) accumulates features up to the m -th stack accounting for the previous $m-1$ residual operations. Despite the complex composition of Ψ and Ξ_{\uparrow} , the fully connected layers in them exhibit Lipschitz continuity [54, Section 6], which ensures the Lipschitz continuity of g^m . From this observation and Remark 3.2, we state the lemma below, with its proof in Appendix A:

Lemma 3.4. *Let $C_{\sigma} > 0$ be given in Definition 3.1. Denote for $m = 1, \dots, M$ by $C_m > 0$ and $C_{m,\uparrow} > 0$ the Lipschitz constants of ψ^m and ξ_{\uparrow}^m , respectively. Then $(\sigma \circ g^m)$ is $C_{\sigma \circ g^m}$ -Lipschitz continuous with*

$$C_{\sigma \circ g^m} = C_{\sigma} C_m (1 + C_m, C_{m,\uparrow})^{L-1} \prod_{n=1}^{m-1} (1 + C_n C_{n,\uparrow})^L, \quad \text{for } m = 2, \dots, M,$$

and $C_{\sigma \circ g^m} = C_{\sigma} C_m (1 + C_m, C_{m,\uparrow})^{L-1}$ for $m = 1$.

By the doubly residual principle, $\{g^m\}_{m=1}^M$ are non-separable with Ψ and Ξ_{\uparrow} . However, the stack-wise alignment via regularizing $\{g^m\}_{m=1}^M$ potentially deteriorates the backcasting power of Ξ_{\uparrow} , which could lead to performance degradation of the model. Instead, we conduct the alignment by regularizing exclusively on feature extractors Ψ . More precisely, this alignment of marginal feature measures from Definition 3.1 is defined as follows: given $\Xi_{\uparrow} = \{\xi_{\uparrow}^m\}_{m=1}^M$,

$$\inf_{\Psi} \left\{ \sum_{m=1}^M \max_{i,j \in \{1, \dots, K\}, i \neq j} d \left((\sigma \circ g^m)_{\#} \mathbb{P}_{\mathcal{X}}^i, (\sigma \circ g^m)_{\#} \mathbb{P}_{\mathcal{X}}^j \right) \right\}, \quad (3.3)$$

where $d(\cdot, \cdot) : \mathcal{P}(\tilde{\mathcal{Z}}) \times \mathcal{P}(\tilde{\mathcal{Z}}) \rightarrow \mathbb{R}_+$ is a divergence or distance between given measures. The illustration of the stack-wise alignment is provided in Figure 2 (in Appendix A).

Note that the third term in Proposition 2.1, i.e., $\max_{i,j \in \{1, \dots, K\}, i \neq j} d_{\mathcal{H}}(\mathbb{P}_{\mathcal{X}}^i, \mathbb{P}_{\mathcal{X}}^j)$, and the stack-wise alignment in (3.3) are perfectly matched once $d(\cdot, \cdot)$ is specified as the \mathcal{H} -divergence. However, the empirical estimation for the \mathcal{H} -divergence is notoriously difficult [5, 6, 31, 51]. These concerns become even more pronounced in the proposed method due to the stack-wise alignment necessitating $MK(K-1)/2$ -times calculation of pairwise divergence, implying heavy computational load. Meanwhile, a substantial body of literature regarding the domain invariant feature learning adopts other alternatives for the \mathcal{H} -divergence, and among them [27, 28, 50, 63], optimal transport distances have been dominant due to their in-depth theoretical ground. In line with this, in the following section, we introduce an optimal transport distance as a relevant choice for $d(\cdot, \cdot)$.

3.2 SINKHORN DIVERGENCE ON MEASURES

In the adversarial framework [20, 50, 59, 63], optimal transport distances have been adopted for training generators to make corresponding push-forward measures close to a given target measure. In particular, the Sinkhorn divergence, an approximate of an entropic regularized optimal transport distance, is shown to be an efficient method to address intensive calculations of divergence between empirical measures [12, 16, 20]. As the stack-wise alignment given in (3.3) leverages on a number of calculations of divergences and hence requires an efficient and accurate toolkit for feasible training, we adopt the Sinkhorn divergence as the relevant one for $d(\cdot, \cdot)$.

To define the Sinkhorn divergence, let us introduce the regularized quadratic Wasserstein-2 distance. To that end, let ϵ be the entropic regularization degree and $\Pi(\mu, \nu; \tilde{\mathcal{Z}})$ is the space of all couplings, i.e., transportation plans, the marginals of which are respectively $\mu, \nu \in \mathcal{P}(\tilde{\mathcal{Z}})$. Then the regularized quadratic Wasserstein-2 distance defined on $\tilde{\mathcal{Z}}$ is defined as follows: for $\epsilon \geq 0$,

$$\mathcal{W}_{\epsilon, \tilde{\mathcal{Z}}}(\mu, \nu) := \inf_{\pi \in \Pi(\mu, \nu; \tilde{\mathcal{Z}})} \left\{ \int_{\tilde{\mathcal{Z}} \times \tilde{\mathcal{Z}}} \left(\|x - y\|^2 + \epsilon \log \left(\frac{d\pi(x, y)}{d\mu(x) d\nu(y)} \right) \right) d\pi(x, y) \right\}. \quad (3.4)$$

By replacing $\tilde{\mathcal{Z}}$ with \mathcal{X} , one can define by $\mathcal{W}_{\epsilon, \mathcal{X}}(\cdot, \cdot)$ the corresponding regularized distance on \mathcal{X} .

The entropic term attached with ϵ in (3.4) is known to improve computational stability of the Wasserstein-2 distance, whereas it causes a bias on corresponding estimator. To alleviate this, according to [11], we adopt the following debiased version of the regularized distance:

Definition 3.5. For $\epsilon \geq 0$, the Sinkhorn divergence is

$$\widehat{\mathcal{W}}_{\epsilon, \tilde{\mathcal{Z}}}(\mu, \nu) := \mathcal{W}_{\epsilon, \tilde{\mathcal{Z}}}(\mu, \nu) - \frac{1}{2} \left(\mathcal{W}_{\epsilon, \tilde{\mathcal{Z}}}(\nu, \nu) + \mathcal{W}_{\epsilon, \tilde{\mathcal{Z}}}(\mu, \mu) \right), \quad \mu, \nu \in \mathcal{P}(\tilde{\mathcal{Z}}). \quad (3.5)$$

Using the duality of the regularized optimal transport distance from [45, Remark 4.18 in Section 4.4] and the Lipschitz continuity of $\{\sigma \circ g^m\}_{m=1}^M$ from Lemma 3.4, we present the following theorem, substantiating the well-definedness and feasibility of our stack-wise alignment via $\widehat{\mathcal{W}}_{\epsilon, \tilde{\mathcal{Z}}}(\cdot, \cdot)$. The proof is provided in Appendix B.

Theorem 3.6. Let $C_{\sigma \circ g^m} > 0$ be as in Lemma 3.4 and define $C := \sum_{m=1}^M \max\{(C_{\sigma \circ g^m})^2, 1\}$. Then the following holds: for $\epsilon \geq 0$,

$$\sum_{m=1}^M \max_{i, j \in \{1, \dots, K\}, i \neq j} \widehat{\mathcal{W}}_{\epsilon, \tilde{\mathcal{Z}}} \left((\sigma \circ g^m)_{\#} \mathbb{P}_{\mathcal{X}}^i, (\sigma \circ g^m)_{\#} \mathbb{P}_{\mathcal{X}}^j \right) \leq C \max_{i, j \in \{1, \dots, K\}, i \neq j} \mathcal{W}_{\epsilon, \mathcal{X}} \left(\mathbb{P}_{\mathcal{X}}^i, \mathbb{P}_{\mathcal{X}}^j \right).$$

In [41, Lemma 3 & Proposition 6], representation learning bounds under the maximum mean discrepancy and the regularized distance in (3.4) are investigated for a single-layered fully connected network. With similar motivation, Theorem 3.6 represents a learning bound for the stack-wise alignment loss under the Sinkhorn divergence as the entropic regularized distance between source domains' measures. While the Lipschitz continuity of $\{\sigma \circ g^m\}_{m=1}^M$ allows a nice bound, there exists room for having a tighter bound by deriving the smallest Lipschitz constant [54] and applying the spectral normalization [37], which will be left for the future extension.

Remark 3.7. Theorem 3.6 supports that the Sinkhorn-based alignment involving intricate doubly residual stacking architecture is feasible, as far as the pair-wise divergence of source domains' measures can be 'a priori' estimated under some suitable divergence (i.e., the entropic regularized Wasserstein distance in the right-hand side of the inequality therein). Indeed, the PoT library introduced by [17] can be used for calculation of the entropic regularized Wasserstein distances. On the other hand, the proposed Sinkhorn-based alignment loss is implemented by `GeomLoss` of [15] that is known to be a significantly efficient and accurate approximate algorithm and will be the main calculation toolkit in the model.

Remark 3.8. For sequential data generation, [59] introduced a causality constraint within optimal transport distances and used Sinkhorn divergence as an approximate for the causality constrained optimal transport distances. However, we do not consider the constraint but adopt Sinkhorn divergence for an approximate of the classic optimal transport distance as in (3.4). This is because unlike the reference, there is no inference for the causality between push-forward feature measures from the source domains.

3.3 TRAINING OBJECTIVE AND ALGORITHM

From Sections 3.1 and 3.2, we define the training objective and corresponding algorithm. To that end, let $\Phi := \{\phi_m\}_{m=1}^M$, $\Theta_{\downarrow} := \{\theta_{m, \downarrow}\}_{m=1}^M$, and $\Theta_{\uparrow} := \{\theta_{m, \uparrow}\}_{m=1}^M$ respectively denote parameters sets of the fully connected neural networks in the residual operators in Ψ , Ξ_{\downarrow} , and Ξ_{\uparrow} given in (2.4). Then corresponding parameterized forms of the operators are respectively given by

$$\Psi(\Phi) = \{\psi^m(\cdot; \phi_m)\}_{m=1}^M, \quad \Xi_{\downarrow}(\Theta_{\downarrow}) = \{\xi_{\downarrow}^m(\cdot; \theta_{m, \downarrow})\}_{m=1}^M, \quad \Xi_{\uparrow}(\Theta_{\uparrow}) = \{\xi_{\uparrow}^m(\cdot; \theta_{m, \uparrow})\}_{m=1}^M.$$

Then denote by $g_{\Phi, \Theta_{\uparrow}}^m := g^m(\cdot; \{\phi_n\}_{n=1}^m, \{\theta_{n, \uparrow}\}_{n=1}^m)$, $m = 1, \dots, M$, the parameterized version of g^m given in (3.2). Let $\mathcal{L}(\mathfrak{F}(\cdot, \cdot, \cdot))$ be the parameterized form of the forecasting loss given in (2.1) and $\mathcal{L}_{\text{align}}(\cdot, \cdot)$ be that of the alignment loss given in (3.3) under the Sinkhorn divergence, i.e.,

$$\mathcal{L}_{\text{align}}(\Phi, \Theta_{\uparrow}) := \sum_{m=1}^M \max_{i, j \in \{1, \dots, K\}, i \neq j} \widehat{\mathcal{W}}_{\epsilon, \tilde{\mathcal{Z}}} \left((\sigma \circ g_{\Phi, \Theta_{\uparrow}}^m)_{\#} \mathbb{P}_{\mathcal{X}}^i, (\sigma \circ g_{\Phi, \Theta_{\uparrow}}^m)_{\#} \mathbb{P}_{\mathcal{X}}^j \right). \quad (3.6)$$

We then provide the following training objective

$$\mathbf{L}_{\lambda}(\Phi, \Theta_{\downarrow}, \Theta_{\uparrow}) := \mathcal{L}(\mathfrak{F}(\Phi, \Theta_{\downarrow}, \Theta_{\uparrow})) + \lambda \mathcal{L}_{\text{align}}(\Phi, \Theta_{\uparrow}). \quad (3.7)$$

To update $(\Phi, \Theta_\downarrow, \Theta_\uparrow)$ according to (3.7), we calculate each divergence $\widehat{\mathcal{W}}_{\epsilon, \tilde{\mathcal{Z}}}((\sigma \circ g_{\Phi, \Theta_\uparrow}^m)_{\#} \mathbb{P}_{\mathcal{X}}^i, (\sigma \circ g_{\Phi, \Theta_\uparrow}^m)_{\#} \mathbb{P}_{\mathcal{X}}^j)$ as its empirical counterpart $\widehat{\mathcal{W}}_{\epsilon, \tilde{\mathcal{Z}}}(\mu_{\Phi, \Theta_\uparrow}^{m, (i)}, \mu_{\Phi, \Theta_\uparrow}^{m, (j)})$, where corresponding empirical measures $\{\mu_{\Phi, \Theta_\uparrow}^{m, (k)}\}_{k=1}^K$ are given as follow: for $k = 1, \dots, K$,

$$\mu_{\Phi, \Theta_\uparrow}^{m, (k)} := \frac{1}{B} \sum_{b=1}^B \delta_{z_b^{(k)}}, \quad \text{with } z_b^{(k)} := \sigma \circ g_{\Phi, \Theta_\uparrow}^m(x_b^{(k)}),$$

where $\{(x_b^{(k)}, y_b^{(k)})\}_{b=1}^B$ are sampled from \mathcal{D}^k , and B and δ_z denote a mini-batch size and the Dirac measure centered on $z \in \tilde{\mathcal{Z}}$, respectively.

As mentioned in Section 3.1, the alignment loss $\mathcal{L}_{\text{align}}(\Phi, \Theta_\uparrow)$ is minimized by updating Φ for given Θ_\uparrow , while $\{g_{\Phi, \Theta_\uparrow}^m\}_{m=1}^M$ are non-separable for Φ and Θ_\uparrow . At the same time, the forecasting loss $\mathcal{L}(\mathfrak{F}(\Phi, \Theta_\downarrow, \Theta_\uparrow))$ is minimized by updating $(\Phi, \Theta_\downarrow, \Theta_\uparrow)$. To bring them together, we adopt the following alternatively updating optimization inspired from [18, Section 3.1]:

$$\Theta_{\downarrow, \Theta_\uparrow}^* := \arg \min_{\Theta_{\downarrow, \Theta_\uparrow}} \mathcal{L}(\mathfrak{F}(\Phi^*, \Theta_{\downarrow, \Theta_\uparrow})) \quad \text{and} \quad \Phi^* := \arg \min_{\Phi} \mathbf{L}_\lambda(\Phi, \Theta_{\downarrow, \Theta_\uparrow}^*). \quad (3.8)$$

The training procedure with this optimization is summarized in Algorithm 1.

Algorithm 1: Training Feature-aligned N-BEATS.

Requires: η (learning rate), B (mini-batch size); Initialize $\Phi, \Theta_\downarrow, \Theta_\uparrow$;

1 **while** not converged **do**

2 Sample $\{(x_b^{(k)}, y_b^{(k)})\}_{b=1}^B$ from \mathcal{D}^k & Initialize $\{\hat{y}_b^{(k)}\}_{b=1}^B \leftarrow 0, k = 1, \dots, K$;

3 **for** $m = 1$ **to** M **do**

4 **for** $k = 1$ **to** K **do**

5 Compute $\{g_{\Phi, \Theta_\uparrow}^m(x_b^{(k)})\}_{b=1}^B$; Update $\hat{y}_b^{(k)} \leftarrow \hat{y}_b^{(k)} + \xi_\downarrow^m (g_{\Phi, \Theta_\uparrow}^m(x_b^{(k)}); \theta_{m, \downarrow}), b = 1, \dots, B$;

6 **end**

7 **end**

8 Compute $\{\mu_{\Phi, \Theta_\uparrow}^{m, (k)}\}_{m=1}^M, k = 1, \dots, K$; Update Φ such that for $m = 1, \dots, M$,

9 $\phi_m \leftarrow \phi_m + \eta \nabla_{\phi_m} \left(\lambda \sum_{n=1}^M \max_{i, j \in \{1, \dots, K\}, i \neq j} \widehat{\mathcal{W}}_{\epsilon, \tilde{\mathcal{Z}}}(\mu_{\Phi, \Theta_\uparrow}^{n, (i)}, \mu_{\Phi, \Theta_\uparrow}^{n, (j)}) \right)$;

10 Update $(\Phi, \Theta_\downarrow, \Theta_\uparrow)$ such that for $m = 1, \dots, M$,

11 $(\phi_m, \theta_{m, \downarrow}, \theta_{m, \uparrow}) \leftarrow (\phi_m, \theta_{m, \downarrow}, \theta_{m, \uparrow}) + \eta \frac{1}{K \cdot B} \sum_{k=1}^K \sum_{b=1}^B \nabla_{(\phi_m, \theta_{m, \downarrow}, \theta_{m, \uparrow})} l(\hat{y}_b^{(k)}, y_b^{(k)})$;

12 **end**

4 EXPERIMENTS

Evaluation details. Our evaluation protocol lies on two principles: (i) real-world scenarios and (ii) examination of various domain shift environments between the source and target domains. For (i), we use financial data from the Federal Reserve Economic Data (FRED) and weather data from the National Centers for Environmental Information (NCEI)¹. For (ii), let us define a set of semantically similar domains as *superdomain* denoted by \mathcal{A}_i , e.g., $i = \text{FRED, NCEI}$. We then categorize the domain shift scenarios into *out-domain generalization* (ODG), *cross-domain generalization* (CDG), and *in-domain generalization* (IDG) such that

- ODG: $\{\mathcal{D}^k\}_{k=1}^K \subseteq \mathcal{A}_i \xrightarrow{\text{Shift } (i \neq j)} \mathcal{D}^T \in \mathcal{A}_j$;
- CDG: $\{\mathcal{D}^k\}_{k=1}^{p-1} \subseteq \mathcal{A}_i, \{\mathcal{D}^k\}_{k=p}^K \subseteq \mathcal{A}_j (2 \leq p \leq K) \xrightarrow{\text{Shift } (i \neq j)} \mathcal{D}^T \in \mathcal{A}_i$ s.t. $\{\mathcal{D}^k\}_{k=1}^{p-1} \cap \mathcal{D}^T = \emptyset$;
- IDG: $\{\mathcal{D}^k\}_{k=1}^K \subseteq \mathcal{A}_i \xrightarrow{\text{Shift } (i=j)} \mathcal{D}^T \in \mathcal{A}_i$ s.t. $\{\mathcal{D}^k\}_{k=1}^K \cap \mathcal{D}^T = \emptyset$.

The domain shift from source to target becomes increasingly pronounced in the sequence of IDG, CDG, and ODG, making it even more challenging to generalize. For detailed data configuration and domain specifications, refer to Appendix C.2.

¹ Refer to <https://fred.stlouisfed.org> (FRED) and <https://ncei.noaa.gov> (NCEI)

Table 1: Domain generalization performance. The performance across all combinations of each ODG, CDG, and IDG scenario are provided (as the average of scenarios for each FRED and NCEI). The notation ‘+ FA’ stands for feature alignment. Each evaluation is conducted three times, with different random seeds. Some stats having values over 10,000 are labeled as ‘NA’.

Methods		N-HiTS	+ FA (Ours)	N-BEATS-I	+ FA (Ours)	N-BEATS-G	+ FA (Ours)	NLinear	DLinear	Autoformer	Informer
ODG											
FRED	SMAPE	0.148	0.134	0.232	0.214	0.172	0.150	0.176	0.307	0.570	1.214
	MASE	0.060	0.057	0.069	0.065	0.061	0.059	48.15	2,214.48	NA	NA
NCEI	SMAPE	0.723	0.713	0.814	0.724	0.722	0.718	1.112	1.302	1.293	1.630
	MASE	0.561	0.512	0.754	0.663	0.561	0.516	2.737	2.869	3.311	5.784
CDG											
FRED	SMAPE	0.124	0.123	0.181	0.179	0.139	0.133	0.176	0.536	0.893	1.143
	MASE	0.058	0.057	0.064	0.062	0.059	0.058	60.929	2,554.27	NA	NA
NCEI	SMAPE	0.742	0.718	0.731	0.718	0.763	0.718	1.096	1.086	1.273	1.437
	MASE	0.581	0.482	0.822	0.755	0.608	0.582	2.734	2.787	3.233	4.147
IDG											
FRED	SMAPE	0.119	0.115	0.137	0.136	0.143	0.119	0.197	0.843	1.001	0.843
	MASE	0.059	0.057	0.062	0.064	0.083	0.058	509.71	1,217.50	NA	NA
NCEI	SMAPE	0.718	0.715	0.713	0.715	0.726	0.714	0.997	0.772	1.268	1.505
	MASE	0.593	0.591	1.011	1.039	0.712	0.591	3.722	3.614	3.573	2.979

Benchmarks. We compare our proposed approach with deep learning based models, including transformer (e.g., Informer [64], Autoformer [58]), MLP-based models (e.g., LTSF-Linear models [60] with NLinear and Dlinear) and N-BEATS based models (e.g., N-BEATS [42] and N-HiTS [9]). Note that since the aforementioned time-series models addressing domain shift [24, 25] still requires target domain data (due to their ‘domain-adapted’ framework), we do not consider their models into our domain-generalized protocol.

Experimental details. We adopt the symmetric mean absolute percentage error (sMAPE) for $\mathcal{L}(\mathfrak{F}(\cdot, \cdot, \cdot))$ given in (3.7) and use the softmax function for σ given in Definition 3.1. The Sinkhorn divergence implemented by `GeomLoss` from [15] is utilized, and ϵ is set to be 0.0025. The Adam optimizer [26] is employed for implementing the optimization given in (3.8). The hyperparameters are set to be $M = 3$, $L = 4$, $\alpha = 50$, $\beta = 10$, and $\gamma = 512$. Others are determined through grid search (detailed in Appendix C.4), and the sMAPE and MASE are adopted as evaluation metrics. Additional implementation details and definitions are provided in Appendix C.

Domain generalization performance. As shown in Table 1, the proposed stack-wise feature alignment significantly improves the domain shift issue within the deep residual stacking architectures with outstanding performance compared to other benchmarks. In particular, we highlight that the improvement is more significant in ODG where the domain shift from source to target is severely pronounced. That being said, the proposed domain-generalized model can perform and adapt well in a very severe situation without any information on the target environment. Other detailed analysis on the results are discussed in Appendix C.5.

Ablation study on divergences. Table 2 provides the ablation results on the choice of divergence (or distances) for the proposed stack-wise feature alignment, in which the benchmarks consist of the classic (not regularized) Wasserstein-2 distance (WD), the maximum mean discrepancy (MMD), and the Kullback–Leibler divergence (KL) and further sensitivity analysis on the Sinkhorn divergence (SD) with respect to $\epsilon > 0$ is also provided. Due to the heavy running cost for implementing WD cases (see Runtime with 314.30 in Table 2) and the training instability associated with KL cases (see Table 6), we consider the target domain case for ‘exchange rate’ (within FRED) and the several source domain scenarios for ODG, CDG and IDG (see Appendix C.2 for the details on the source domains’ combinations). For the same reasons, the baseline model is fixed to N-BEATS-G. The entire results (except for WD cases) are provided in Tables 6 and 7.

Table 2: Ablation study on divergences. Runtime is measured for a single iteration.

Divergences		WD	SD ($\epsilon > 0$)			MMD	KL
			1e-5	2.5e-3	1e-1		
ODG	SMAPE	0.031	0.040	0.032	0.033	0.035	0.045
	MASE	0.022	0.059	0.022	0.022	0.055	0.057
CDG	SMAPE	0.028	0.026	0.028	0.027	0.029	0.030
	MASE	0.039	0.058	0.040	0.039	0.041	0.039
IDG	SMAPE	0.024	0.024	0.024	0.025	0.025	0.026
	MASE	0.049	0.050	0.050	0.050	0.051	0.049
Runtime (sec)		314.30	0.68			0.81	0.53

As the Sinkhorn divergence is an accurate approximate of the Wasserstein-2 distance (see Definition 3.5), the similar results for the two cases in Table 2 seem to be reasonable. On the other hand, their

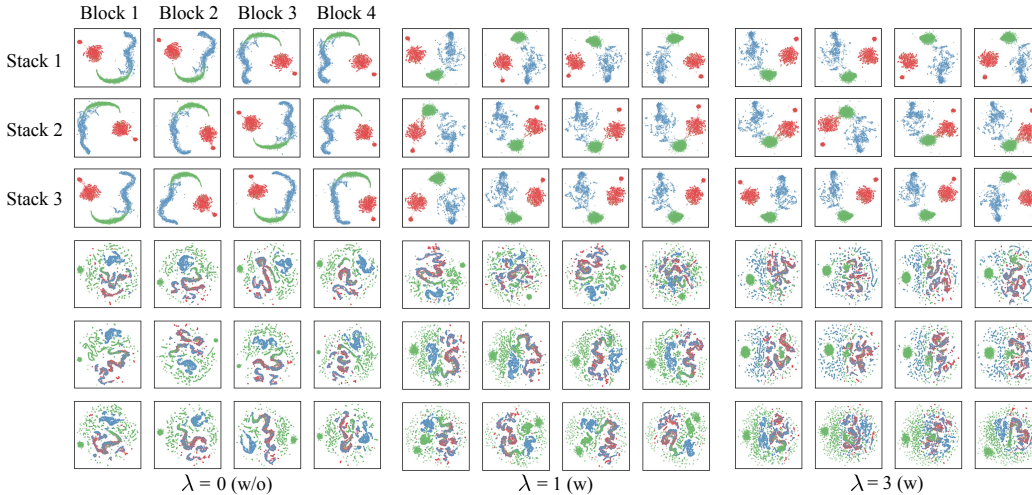


Figure 1: Visualization on invariant feature learning. In the aligned scenario (w), the interconnection between green and red instances, particularly at $\lambda = 3$, becomes visible. Contrastingly, in the non-aligned scenario (w/o), we observe a pronounced dispersion, especially of the blue instances within the initial two stacks at $\lambda = 3$, resulting in heightened inter-domain entropy.

computational costs are incomparable. That being said, the Sinkhorn divergence is the computationally feasible and accurate toolkit for the proposed stack-wise alignment with optimal transport based divergence, while some instability issue (see [4, 20]) would come out for extremely small $\epsilon > 0$ (i.e., $\epsilon = 1e-5$ in Table 2). In comparison with the MMD and KL cases (see Tables 6 and 7 as well for the entire results), the Sinkhorn divergence case seems to be marginally better but shows more stable and consistent results in overall domain shift scenarios. From these empirical evidences, we hence conclude that the choice of the Sinkhorn divergence allows the model to bring both the abundant theoretical advantages of optimal transport problems and the practical feasibility.

Visualization on invariant feature learning. To visualize representations, i.e., samples of marginal feature measures observed from N-BEATS-G with and without alignment, we use the uniform manifold approximation and projection (UMAP) introduced by [36]. To minimize the effect of unaligned scale information, the softmax function is employed to remove the scale information and instead emphasize the semantic relationship across domains. As illustrated in Figure 1, we observe the proximity between instances and the substantial upsurge in the entropy of domains. For other cases on N-BEATS-I and N-HiTS, please refer to Figure 5 in Appendix D.

Other results. On top of the aforementioned results, further experiments are provided in Appendix E, which supports our choices and assumptions on the proposed model. The followings summarize the corresponding results:

- Comparison of stack-wise and block-wise feature alignment (Appendix E.1);
- Comparison of several normalization functions (Appendix E.2);
- Evaluation of the model under marginal (or the absence of) domain shift (Appendix E.3).

5 DISCUSSION AND EXTENSIONS

There are some unresolved theoretical parts in the current article such as a convergence analysis for the training loss (given in (3.8)) with the empirical risk minimization and the stack-wise feature alignment, filling the gap between the Sinkhorn divergence and the \mathcal{H} -divergence adopted in the error analysis of domain generalization models (given in Proposition 2.1), and the instability issue coming from the small entropic parameter $\epsilon > 0$ in the Sinkhorn divergence (see Table 2).

On the other hand, there are many rooms for an extension of the proposed domain-generalized time-series forecasting model such as the ‘conditional’ feature measure alignment in [62] and ‘adversarial representation learning framework’ in [29]. Moreover, considering the utilization of ‘moments’ as

distribution measurements in [21] and mitigating distribution mismatches through the ‘contrastive loss’ in [38] would represent meaningful avenues for future research.

Acknowledgement. K. Park acknowledges the support of the Presidential Postdoctoral Fellowship 2023 of Nanyang Technological University. M. Kang was supported by the NRF grant [2021R1A2C3010887] and the MSIT/IITP([1711117093], [NO.2021-0-00077], [No. 2021-0-01343, Artificial Intelligence Graduate School Program (SNU)]).

REFERENCES

- [1] I. Albuquerque, J. Monteiro, M. Darvishi, T. H. Falk, and I. Mitliagkas. Generalizing to unseen domains via distribution matching. *arXiv preprint arXiv:1911.00804*, 2019.
- [2] L. Ambrosio, N. Gigli, and G. Savaré. *Gradient flows: in metric spaces and in the space of probability measures*. Springer Science & Business Media, 2005.
- [3] K. Bandara, C. Bergmeir, and S. Smyl. Forecasting across time series databases using recurrent neural networks on groups of similar series: A clustering approach. *Expert Systems with Applications*, 140:112896, 2020.
- [4] H. Bao and S. Sakaue. Sparse regularized optimal transport with deformed q-entropy. *Entropy*, 24(11):1634, 2022.
- [5] S. Ben-David, J. Blitzer, K. Crammer, A. Kulesza, F. Pereira, and J. W. Vaughan. A theory of learning from different domains. *Machine learning*, 79:151–175, 2010.
- [6] S. Ben-David, J. Blitzer, K. Crammer, and F. Pereira. Analysis of representations for domain adaptation. *Advances in neural information processing systems*, 19, 2006.
- [7] Y. Bengio, A. Courville, and P. Vincent. Representation learning: A review and new perspectives. *IEEE Transactions on Pattern Analysis and Machine Intelligence*, 35(8):1798–1828, 2013.
- [8] W. Cao, D. Wang, J. Li, H. Zhou, L. Li, and Y. Li. Brits: Bidirectional recurrent imputation for time series. *Advances in Neural Information Processing Systems*, 31, 2018.
- [9] C. Challu, K. G. Olivares, B. N. Oreshkin, F. Garza, M. Mergenthaler, and A. Dubrawski. N-hits: Neural hierarchical interpolation for time series forecasting. *arXiv preprint arXiv:2201.12886*, 2022.
- [10] Y. Chen, Y. Kang, Y. Chen, and Z. Wang. Probabilistic forecasting with temporal convolutional neural network. *Neurocomputing*, 399:491–501, 2020.
- [11] L. Chizat, P. Roussillon, F. Léger, F.-X. Vialard, and G. Peyré. Faster wasserstein distance estimation with the sinkhorn divergence. *Advances in Neural Information Processing Systems*, 33:2257–2269, 2020.
- [12] S. Di Marino and A. Gerolin. Optimal transport losses and sinkhorn algorithm with general convex regularization. *arXiv preprint arXiv:2007.00976*, 2020.
- [13] R. M. Dudley. The speed of mean glivenko-cantelli convergence. *The Annals of Mathematical Statistics*, 40(1):40–50, 1969.
- [14] H. Federer. *Geometric measure theory*. Springer, 2014.
- [15] J. Feydy. Geometric data analysis, beyond convolutions. *Applied Mathematics*, 2020.
- [16] J. Feydy, T. Séjourné, F.-X. Vialard, S.-i. Amari, A. Trouvé, and G. Peyré. Interpolating between optimal transport and mmd using sinkhorn divergences. In *The 22nd International Conference on Artificial Intelligence and Statistics*, pages 2681–2690. PMLR, 2019.
- [17] R. Flamary, N. Courty, A. Gramfort, M. Z. Alaya, A. Boisbunon, S. Chambon, L. Chapel, A. Corenflos, K. Fatras, N. Fournier, et al. Pot: Python optimal transport. *The Journal of Machine Learning Research*, 22(1):3571–3578, 2021.

- [18] Y. Ganin and V. Lempitsky. Unsupervised domain adaptation by backpropagation. In *International Conference on Machine Learning*, pages 1180–1189. PMLR, 2015.
- [19] Y. Ganin, E. Ustinova, H. Ajakan, P. Germain, H. Larochelle, F. Laviolette, M. Marchand, and V. Lempitsky. Domain-adversarial training of neural networks. *The Journal of Machine Learning Research*, 17(1):2096–2030, 2016.
- [20] A. Genevay, G. Peyré, and M. Cuturi. Learning generative models with sinkhorn divergences. In *International Conference on Artificial Intelligence and Statistics*, pages 1608–1617. PMLR, 2018.
- [21] M. Ghifary, D. Balduzzi, W. B. Kleijn, and M. Zhang. Scatter component analysis: A unified framework for domain adaptation and domain generalization. *IEEE transactions on pattern analysis and machine intelligence*, 39(7):1414–1430, 2016.
- [22] A. Gretton, K. M. Borgwardt, M. J. Rasch, B. Schölkopf, and A. Smola. A kernel two-sample test. *The Journal of Machine Learning Research*, 13(1):723–773, 2012.
- [23] H. Hewamalage, C. Bergmeir, and K. Bandara. Recurrent neural networks for time series forecasting: Current status and future directions. *International Journal of Forecasting*, 37(1):388–427, 2021.
- [24] H. Hu, M. Tang, and C. Bai. Datsing: Data augmented time series forecasting with adversarial domain adaptation. In *Proceedings of the ACM International Conference on Information & Knowledge Management*, pages 2061–2064, 2020.
- [25] X. Jin, Y. Park, D. Maddix, H. Wang, and Y. Wang. Domain adaptation for time series forecasting via attention sharing. In *International Conference on Machine Learning*, pages 10280–10297. PMLR, 2022.
- [26] D. P. Kingma and J. Ba. Adam: A method for stochastic optimization. *arXiv preprint arXiv:1412.6980*, 2014.
- [27] T.-N. Le, A. Habrard, and M. Sebban. Deep multi-wasserstein unsupervised domain adaptation. *Pattern Recognition Letters*, 125:249–255, 2019.
- [28] C.-Y. Lee, T. Batra, M. H. Baig, and D. Ulbricht. Sliced wasserstein discrepancy for unsupervised domain adaptation. In *Proceedings of the IEEE/CVF conference on computer vision and pattern recognition*, pages 10285–10295, 2019.
- [29] H. Li, S. J. Pan, S. Wang, and A. C. Kot. Domain generalization with adversarial feature learning. In *Proceedings of the IEEE Conference on Computer Vision and Pattern Recognition*, pages 5400–5409, 2018.
- [30] Y. Li, D. E. Carlson, et al. Extracting relationships by multi-domain matching. *Advances in neural information processing systems*, 31, 2018.
- [31] Y. Li, X. Tian, M. Gong, Y. Liu, T. Liu, K. Zhang, and D. Tao. Deep domain generalization via conditional invariant adversarial networks. In *Proceedings of the European Conference on Computer Vision*, pages 624–639, 2018.
- [32] B. Lim, S. Ö. Arık, N. Loeff, and T. Pfister. Temporal fusion transformers for interpretable multi-horizon time series forecasting. *International Journal of Forecasting*, 37(4):1748–1764, 2021.
- [33] M. Liu, A. Zeng, M. Chen, Z. Xu, Q. Lai, L. Ma, and Q. Xu. Scinet: time series modeling and forecasting with sample convolution and interaction. *Advances in Neural Information Processing Systems*, 35:5816–5828, 2022.
- [34] K. Madhusudhanan, J. Burchert, N. Duong-Trung, S. Born, and L. Schmidt-Thieme. Yformer: U-net inspired transformer architecture for far horizon time series forecasting. *arXiv preprint arXiv:2110.08255*, 2021.

- [35] T. Matsuura and T. Harada. Domain generalization using a mixture of multiple latent domains. In *Proceedings of the AAAI Conference on Artificial Intelligence*, volume 34, pages 11749–11756, 2020.
- [36] L. McInnes, J. Healy, and J. Melville. Umap: Uniform manifold approximation and projection for dimension reduction. *arXiv preprint arXiv:1802.03426*, 2018.
- [37] T. Miyato, T. Kataoka, M. Koyama, and Y. Yoshida. Spectral normalization for generative adversarial networks. *arXiv preprint arXiv:1802.05957*, 2018.
- [38] S. Motiian, M. Piccirilli, D. A. Adjeroh, and G. Doretto. Unified deep supervised domain adaptation and generalization. In *Proceedings of the IEEE international conference on computer vision*, pages 5715–5725, 2017.
- [39] K. Muandet, D. Balduzzi, and B. Schölkopf. Domain generalization via invariant feature representation. In *International Conference on Machine Learning*, pages 10–18. PMLR, 2013.
- [40] V. Nair and G. E. Hinton. Rectified linear units improve restricted boltzmann machines. In *International Conference on Machine Learning*, pages 807–814, 2010.
- [41] L. Oneto, M. Donini, G. Luise, C. Ciliberto, A. Maurer, and M. Pontil. Exploiting mmd and sinkhorn divergences for fair and transferable representation learning. *Advances in Neural Information Processing Systems*, 33:15360–15370, 2020.
- [42] B. N. Oreshkin, D. Carпов, N. Chapados, and Y. Bengio. N-beats: Neural basis expansion analysis for interpretable time series forecasting. *arXiv preprint arXiv:1905.10437*, 2019.
- [43] B. N. Oreshkin, D. Carпов, N. Chapados, and Y. Bengio. Meta-learning framework with applications to zero-shot time-series forecasting. In *Proceedings of the AAAI Conference on Artificial Intelligence*, volume 35, pages 9242–9250, 2021.
- [44] R. Pascanu, T. Mikolov, and Y. Bengio. On the difficulty of training recurrent neural networks. In *International conference on machine learning*, pages 1310–1318. Pmlr, 2013.
- [45] G. Peyré, M. Cuturi, et al. Computational optimal transport: With applications to data science. *Foundations and Trends® in Machine Learning*, 11(5-6):355–607, 2019.
- [46] J. Quinonero-Candela, M. Sugiyama, A. Schwaighofer, and N. D. Lawrence. *Dataset shift in machine learning*. Mit Press, 2008.
- [47] A. Ramdas, N. García Trillos, and M. Cuturi. On wasserstein two-sample testing and related families of nonparametric tests. *Entropy*, 19(2):47, 2017.
- [48] S. S. Rangapuram, M. W. Seeger, J. Gasthaus, L. Stella, Y. Wang, and T. Januschowski. Deep state space models for time series forecasting. *Advances in Neural Information Processing Systems*, 31, 2018.
- [49] D. Salinas, V. Flunkert, J. Gasthaus, and T. Januschowski. Deepar: Probabilistic forecasting with autoregressive recurrent networks. *International Journal of Forecasting*, 36(3):1181–1191, 2020.
- [50] J. Shen, Y. Qu, W. Zhang, and Y. Yu. Wasserstein distance guided representation learning for domain adaptation. In *Proceedings of the AAAI Conference on Artificial Intelligence*, volume 32, 2018.
- [51] C. Shui, Q. Chen, J. Wen, F. Zhou, C. Gagné, and B. Wang. A novel domain adaptation theory with jensen–shannon divergence. *Knowledge-Based Systems*, 257:109808, 2022.
- [52] C. Shui, B. Wang, and C. Gagné. On the benefits of representation regularization in invariance based domain generalization. *Machine Learning*, 111(3):895–915, 2022.
- [53] V. Vapnik. Principles of risk minimization for learning theory. *Advances in Neural Information Processing Systems*, 4, 1991.

- [54] A. Virmaux and K. Scaman. Lipschitz regularity of deep neural networks: analysis and efficient estimation. *Advances in Neural Information Processing Systems*, 31, 2018.
- [55] J. Wang, C. Lan, C. Liu, Y. Ouyang, T. Qin, W. Lu, Y. Chen, W. Zeng, and P. Yu. Generalizing to unseen domains: A survey on domain generalization. *IEEE Transactions on Knowledge and Data Engineering*, 2022.
- [56] M. Wang and W. Deng. Deep visual domain adaptation: A survey. *Neurocomputing*, 312:135–153, 2018.
- [57] G. Woo, C. Liu, D. Sahoo, A. Kumar, and S. Hoi. Etsformer: Exponential smoothing transformers for time-series forecasting. *arXiv preprint arXiv:2202.01381*, 2022.
- [58] H. Wu, J. Xu, J. Wang, and M. Long. Autoformer: Decomposition transformers with auto-correlation for long-term series forecasting. *Advances in Neural Information Processing Systems*, 34:22419–22430, 2021.
- [59] T. Xu, L. K. Wenliang, M. Munn, and B. Acciaio. Cot-gan: Generating sequential data via causal optimal transport. *Advances in neural information processing systems*, 33:8798–8809, 2020.
- [60] A. Zeng, M. Chen, L. Zhang, and Q. Xu. Are transformers effective for time series forecasting? *arXiv preprint arXiv:2205.13504*, 2022.
- [61] H. Zhao, R. T. Des Combes, K. Zhang, and G. Gordon. On learning invariant representations for domain adaptation. In *International Conference on Machine Learning*, pages 7523–7532. PMLR, 2019.
- [62] S. Zhao, M. Gong, T. Liu, H. Fu, and D. Tao. Domain generalization via entropy regularization. *Advances in Neural Information Processing Systems*, 33:16096–16107, 2020.
- [63] F. Zhou, Z. Jiang, C. Shui, B. Wang, and B. Chaib-draa. Domain generalization via optimal transport with metric similarity learning. *Neurocomputing*, 456:469–480, 2021.
- [64] H. Zhou, S. Zhang, J. Peng, S. Zhang, J. Li, H. Xiong, and W. Zhang. Informer: Beyond efficient transformer for long sequence time-series forecasting. In *Proceedings of the AAAI Conference on Artificial Intelligence*, volume 35, pages 11106–11115, 2021.
- [65] T. Zhou, Z. Ma, Q. Wen, X. Wang, L. Sun, and R. Jin. Fedformer: Frequency enhanced decomposed transformer for long-term series forecasting. In *International Conference on Machine Learning*, pages 27268–27286. PMLR, 2022.

APPENDIX

A DETAILS ON SECTIONS 2.2 AND 3.1

The m -th residual operators $(\psi^m, \xi_{\downarrow}^m, \xi_{\uparrow}^m) \in \Psi \times \Xi_{\downarrow} \times \Xi_{\uparrow}$, $m = 1, \dots, M$, are given by

$$\begin{aligned} \psi^m(x) &:= (\text{FC}^{m,N} \circ \text{FC}^{m,N-1} \dots \circ \text{FC}^{m,1})(x), & x \in \mathcal{X} = \mathbb{R}^{\alpha}, \\ \xi_{\downarrow}^m(z) &:= \mathbf{V}_{m,\downarrow} \mathbf{W}_{m,\downarrow} z, & z \in \mathcal{Z} = \mathbb{R}^{\gamma}, \\ \xi_{\uparrow}^m(z) &:= \mathbf{V}_{m,\uparrow} \mathbf{W}_{m,\uparrow} z, & z \in \mathcal{Z} = \mathbb{R}^{\gamma}. \end{aligned} \quad (\text{A.1})$$

These operators correspond to the m -th stack and involve fully connected layers denoted by $\text{FC}^{m,n}$ with RELU activation function [40]. Specifically, $\text{FC}^{m,n}(x)$ is defined as $\text{RELU}(\mathbf{W}_{m,n}x + \mathbf{b}_{m,n})$, where $\mathbf{W}_{m,n}$ and $\mathbf{b}_{m,n}$ are trainable weight and bias parameters, respectively. The matrix $\mathbf{W}_{m,\downarrow} \in \mathbb{R}^{\gamma_{\downarrow} \times \gamma}$ (resp. $\mathbf{W}_{m,\uparrow} \in \mathbb{R}^{\gamma_{\uparrow} \times \gamma}$) represents a trainable linear projection layer for forecasting (resp. backcasting) operations. For the parameters β , α , and γ denoting to the forecast horizon, lookback horizon, and latent space dimension, respectively, $\mathbf{V}_{m,\downarrow} \in \mathbb{R}^{\beta \times \gamma_{\downarrow}}$ (resp. $\mathbf{V}_{m,\uparrow} \in \mathbb{R}^{\alpha \times \gamma_{\uparrow}}$) represents a forecast basis (resp. backcast basis) matrix, given by

$$\begin{aligned} \mathbf{V}_{m,\downarrow} &:= (\mathbf{v}_{m,\downarrow}^1, \dots, \mathbf{v}_{m,\downarrow}^{\gamma_{\downarrow}}) \in \mathbb{R}^{\beta \times \gamma_{\downarrow}} \quad \text{with} \quad \mathbf{v}_{m,\downarrow}^1, \dots, \mathbf{v}_{m,\downarrow}^{\gamma_{\downarrow}} \in \mathbb{R}^{\beta}, \\ (\text{resp. } \mathbf{V}_{m,\uparrow} &:= (\mathbf{v}_{m,\uparrow}^1, \dots, \mathbf{v}_{m,\uparrow}^{\gamma_{\uparrow}}) \in \mathbb{R}^{\alpha \times \gamma_{\uparrow}} \quad \text{with} \quad (\mathbf{v}_{m,\uparrow}^1, \dots, \mathbf{v}_{m,\uparrow}^{\gamma_{\uparrow}}) \in \mathbb{R}^{\alpha}), \end{aligned} \quad (\text{A.2})$$

and each $\mathbf{v}_{m,\downarrow}^i$ (resp. $\mathbf{v}_{m,\uparrow}^i$), is a forecast basis (resp. backcast basis) vector.

Note that $\mathbf{V}_{m,\downarrow}$ and $\mathbf{V}_{m,\uparrow}$ are set to be non-trainable parameter sets that embrace vital information for time series forecasting purposes, including trends and seasonality. These parameter sets are based on [42]. The basis expansion representations in (A.1) with flexible adjustments in (A.2) allow the model to capture the relevant patterns in the sequential data.

The main difference between N-BEATS-G and N-BEATS-I lies on the utilization of $\mathbf{V}_{m,\downarrow}$ and $\mathbf{V}_{m,\uparrow}$. More precisely, N-BEATS-G does not incorporate any specialized time series-specific knowledge but employs the identity matrices for $\mathbf{V}_{m,\downarrow}$ and $\mathbf{V}_{m,\uparrow}$. In contrast, N-BEATS-I captures trend and seasonality information, which derives the interpretability. Specifically, $\mathbf{V}_{m,\downarrow}$ is given by $\mathbf{V}_{m,\downarrow} = (\mathbf{1}, \mathbf{t}, \dots, \mathbf{t}^{\gamma_{\downarrow}})$, where $\mathbf{t} = \frac{1}{\beta}(0, 1, 2, \dots, \beta - 2, \beta - 1)^{\top}$. This choice is motivated by the characteristic of trends, which are typically represented by monotonic or slowly varying functions. For the seasonality, $\mathbf{V}_{m,\downarrow}$ is defined using a periodic function, (specifically the Fourier series), so that $\mathbf{V}_{m,\downarrow} = (\mathbf{1}, \cos(2\pi\mathbf{t}), \dots, \cos(2\pi\lfloor\beta/2 - 1\rfloor\mathbf{t}), \sin(2\pi\mathbf{t}), \dots, \sin(2\pi\lfloor\beta/2 - 1\rfloor\mathbf{t}))^{\top}$. The dimension of $\mathbf{V}_{m,\downarrow}$ is determined by adjusting the interval between $\cos(2\pi\mathbf{t})$ and $\cos(2\pi\lfloor\beta/2 - 1\rfloor\mathbf{t})$, as well as $\sin(2\pi\mathbf{t})$ and $\sin(2\pi\lfloor\beta/2 - 1\rfloor\mathbf{t})$. This formulation incorporates the notion of sinusoidal waveforms to capture the periodic nature of seasonality. The formulation of $\mathbf{V}_{m,\uparrow}$ is identical to that of $\mathbf{V}_{m,\downarrow}$, with the only difference being the replacement of α with β and γ_{\downarrow} with γ_{\uparrow} .

Since each ψ^m defined in (A.1) is an N -layered fully connected network with the 1-Lipschitz continuous activation, i.e., RELU, we can apply [54, Section 6] to have an explicit representation for the (Rademacher) Lipschitz constant $C_m > 0$ of ψ^m [14, Theorem 3.1.6]. Furthermore, the forecasting and backcasting operators, ξ_{\downarrow}^m and ξ_{\uparrow}^m , are matrix operators, and we can calculate their Lipschitz constants $C_{m,\downarrow}$ and $C_{m,\uparrow}$ by using the matrix norm induced by the Euclidean norm $\|\cdot\|$, i.e., $C_{m,\downarrow} := \|\mathbf{V}_{m,\downarrow} \mathbf{W}_{m,\downarrow}\| > 0$ and $C_{m,\uparrow} := \|\mathbf{V}_{m,\uparrow} \mathbf{W}_{m,\uparrow}\| > 0$.

Proof of Lemma 3.4. From the definition of $\sigma \circ g^m$ in Definition 3.1 and the Lipschitz continuity of σ and ψ^m with corresponding constants $C_{\sigma} > 0$ and $C_m > 0$, it follows for every $m = 1, \dots, M$, that for any $x, y \in \mathcal{X}$,

$$\begin{aligned} \|\sigma \circ g^m(x) - \sigma \circ g^m(y)\| &\leq C_{\sigma} \|g^m(x) - g^m(y)\| \\ &\leq C_{\sigma} C_m \left\| \left((r^m)^{(L-1)} \circ (r^{m-1})^{(L)} \circ \dots \circ (r^1)^{(L)} \right)(x) \right. \\ &\quad \left. - \left((r^m)^{(L-1)} \circ (r^{m-1})^{(L)} \circ \dots \circ (r^1)^{(L)} \right)(y) \right\|. \end{aligned} \quad (\text{A.3})$$

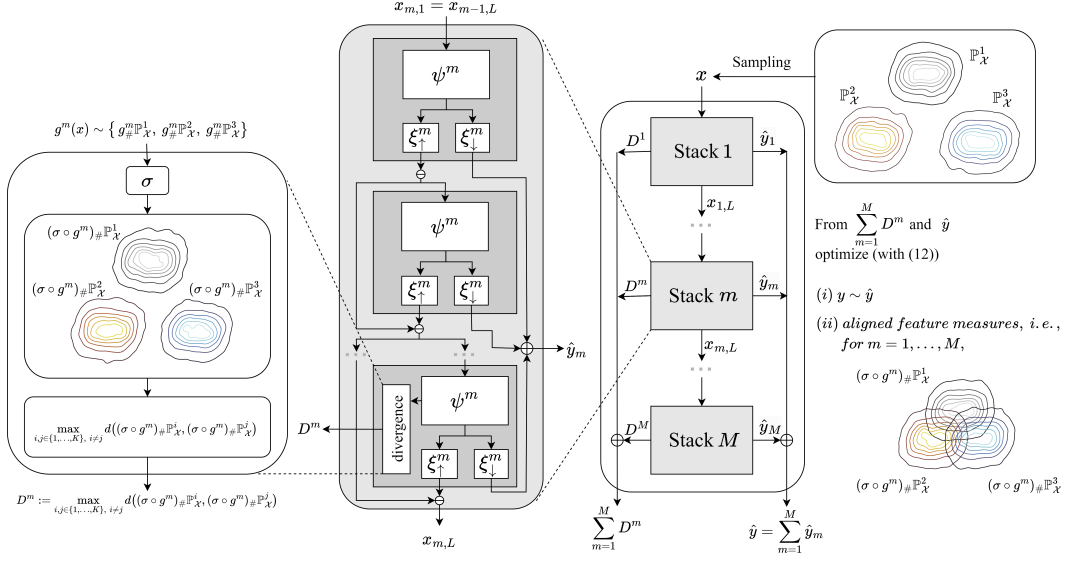


Figure 2: Illustration of Feature-aligned N-BEATS.

Based on the residual operation in (3.1), i.e., $r^m(x) = x - (\xi_{\uparrow}^m \circ \psi^m)(x)$, and considering the Lipschitz continuity of σ and ψ^m with respective constants $C_{\sigma} > 0$ and $C_m > 0$, we can establish the following inequality for every $m = 1, \dots, M$, and any $x, y \in \mathcal{X}$,

$$\|r^m(x) - r^m(y)\| \leq \|x - y\| + \|(\xi_{\uparrow}^m \circ \psi^m)(x) - (\xi_{\uparrow}^m \circ \psi^m)(y)\| \leq (1 + C_{m,\uparrow} C_m) \|x - y\|.$$

Applying this to $L - 1$ -times composition of r^m , i.e., $(r^m)^{(L-1)}$, we have that for any $x, y \in \mathcal{X}$,

$$\|(r^m)^{(L-1)}(x) - (r^m)^{(L-1)}(y)\| \leq (1 + C_{m,\uparrow} C_m)^{L-1} \|x - y\|.$$

Using the same arguments for the remaining compositions $(r^{m-1})^{(L)}$, $(r^{m-2})^{(L)}$, \dots , $(r^1)^{(L)}$ in (A.3), we deduce that for any $x, y \in \mathcal{X}$,

$$\|\sigma \circ g^m(x) - \sigma \circ g^m(y)\| \leq C_{\sigma} C_m (1 + C_m C_{m,\uparrow})^{L-1} \prod_{n=1}^{m-1} (1 + C_n C_{n,\uparrow})^L \|x - y\|.$$

□

B DETAILS ON SECTION 3.2

Proof of Theorem 3.6. We first note that from the nonnegativity of the entropy term in the regularized Wasserstein distance $\mathcal{W}_{\epsilon, \tilde{\mathcal{Z}}}$, i.e., for every $\pi \in \Pi(\mu, \nu; \tilde{\mathcal{Z}})$,

$$\int_{\tilde{\mathcal{Z}} \times \tilde{\mathcal{Z}}} \epsilon \log \left(\frac{d\pi(x, y)}{d\mu(x) d\nu(y)} \right) d\pi(x, y) \geq 0,$$

it is clear that $\mathcal{W}_{\epsilon, \tilde{\mathcal{Z}}}(\mu, \nu) \geq 0$ for every $\mu, \nu \in \mathcal{P}(\tilde{\mathcal{Z}})$. Moreover, from the definition of $\widehat{\mathcal{W}}_{\epsilon, \tilde{\mathcal{Z}}}$, i.e., $\widehat{\mathcal{W}}_{\epsilon, \tilde{\mathcal{Z}}}(\mu, \nu) = \mathcal{W}_{\epsilon, \tilde{\mathcal{Z}}}(\mu, \nu) - \frac{1}{2}(\mathcal{W}_{\epsilon, \tilde{\mathcal{Z}}}(\nu, \nu) + \mathcal{W}_{\epsilon, \tilde{\mathcal{Z}}}(\mu, \mu))$, for $\mu, \nu \in \mathcal{P}(\tilde{\mathcal{Z}})$, it follows that for every $m = 1, \dots, M$ and any $i, j \in \{1, \dots, K\}$ such that $i \neq j$,

$$\widehat{\mathcal{W}}_{\epsilon, \tilde{\mathcal{Z}}}((\sigma \circ g^m)_{\#} \mathbb{P}_{\mathcal{X}}^i, (\sigma \circ g^m)_{\#} \mathbb{P}_{\mathcal{X}}^j) \leq \mathcal{W}_{\epsilon, \tilde{\mathcal{Z}}}((\sigma \circ g^m)_{\#} \mathbb{P}_{\mathcal{X}}^i, (\sigma \circ g^m)_{\#} \mathbb{P}_{\mathcal{X}}^j). \quad (\text{B.1})$$

Let $\mathcal{C}(\tilde{\mathcal{Z}})$ be the set of all real-valued continuous functions on $\tilde{\mathcal{Z}}$ and $\mathcal{C}(\mathcal{X}; \sigma \circ g^m)$ be defined by

$$\mathcal{C}(\mathcal{X}; \sigma \circ g^m) := \{f : \mathcal{X} \rightarrow \mathbb{R} \mid \exists \tilde{f} \in \mathcal{C}(\tilde{\mathcal{Z}}) \text{ s.t. } f = \tilde{f} \circ \sigma \circ g^m\}.$$

Then, from the dual representation in [45, Remark 4.18 in Section 4.4] based on the Lagrangian method and the integral property of push-forward measures in [2, Section 5.2], it follows for every $m = 1, \dots, M$ that given $\mathbb{P}_{\mathcal{X}}^i, \mathbb{P}_{\mathcal{X}}^j \in \{\mathbb{P}_{\mathcal{X}}^k\}_{k=1}^K$ with $i \neq j$,

$$\begin{aligned}
& \mathcal{W}_{\epsilon, \tilde{\mathcal{Z}}}((\sigma \circ g^m)_{\#} \mathbb{P}_{\mathcal{X}}^i, (\sigma \circ g^m)_{\#} \mathbb{P}_{\mathcal{X}}^j) \\
&= \sup_{\tilde{f}, \tilde{h} \in \mathcal{C}(\tilde{\mathcal{Z}})} \left\{ \int_{\tilde{\mathcal{Z}}} \tilde{f}(x) d((\sigma \circ g^m)_{\#} \mathbb{P}_{\mathcal{X}}^i)(x) + \int_{\tilde{\mathcal{Z}}} \tilde{h}(y) d((\sigma \circ g^m)_{\#} \mathbb{P}_{\mathcal{X}}^j)(y) \right. \\
&\quad \left. - \epsilon \int_{\tilde{\mathcal{Z}} \times \tilde{\mathcal{Z}}} e^{\frac{1}{\epsilon}(\tilde{f}(x) + \tilde{h}(y) - \|x - y\|^2)} d((\sigma \circ g^m)_{\#} \mathbb{P}_{\mathcal{X}}^i) \otimes ((\sigma \circ g^m)_{\#} \mathbb{P}_{\mathcal{X}}^j)(x, y) \right\} \quad (\text{B.2}) \\
&= \sup_{f, h \in \mathcal{C}(\mathcal{X}; \sigma \circ g^m)} \left\{ \int_{\mathcal{X}} f(x) d\mathbb{P}_{\mathcal{X}}^i(x) + \int_{\mathcal{X}} h(y) d\mathbb{P}_{\mathcal{X}}^j(y) \right. \\
&\quad \left. - \epsilon \int_{\mathcal{X} \times \mathcal{X}} e^{\frac{1}{\epsilon}(f(x) + h(y) - \|(\sigma \circ g^m)(x) - (\sigma \circ g^m)(y)\|^2)} d(\mathbb{P}_{\mathcal{X}}^i \otimes \mathbb{P}_{\mathcal{X}}^j)(x, y) \right\}.
\end{aligned}$$

Consider the following regularized optimal transport problem:

$$\begin{aligned}
\tilde{\mathcal{W}}_{\epsilon, \mathcal{X}}(\mathbb{P}^i, \mathbb{P}^j; \sigma \circ g^m) &:= \inf_{\pi \in \Pi(\mathbb{P}^i, \mathbb{P}^j; \mathcal{X})} \left\{ \int_{\mathcal{X} \times \mathcal{X}} (\|\sigma \circ g^m(x) - \sigma \circ g^m(y)\|^2 \right. \\
&\quad \left. + \epsilon \log \left(\frac{d\pi(x, y)}{d\mathbb{P}_{\mathcal{X}}^i(x) d\mathbb{P}_{\mathcal{X}}^j(y)} \right) \right\}.
\end{aligned}$$

Then, from the dual representation, as in (B.2), it follows that

$$\begin{aligned}
\tilde{\mathcal{W}}_{\epsilon, \mathcal{X}}(\mathbb{P}^i, \mathbb{P}^j; \sigma \circ g^m) &= \sup_{f, h \in \mathcal{C}(\mathcal{X})} \left\{ \int_{\mathcal{X}} f(x) d\mathbb{P}_{\mathcal{X}}^i(x) + \int_{\mathcal{X}} h(y) d\mathbb{P}_{\mathcal{X}}^j(y) \right. \\
&\quad \left. - \epsilon \int_{\mathcal{X} \times \mathcal{X}} e^{\frac{1}{\epsilon}(f(x) + h(y) - \|(\sigma \circ g^m)(x) - (\sigma \circ g^m)(y)\|^2)} d(\mathbb{P}_{\mathcal{X}}^i \otimes \mathbb{P}_{\mathcal{X}}^j)(x, y) \right\}, \quad (\text{B.3})
\end{aligned}$$

where $\mathcal{C}(\mathcal{X})$ denotes the set of all continuous real-valued functions on \mathcal{X} . From the dual representations in (B.2) and (B.3) and the relation that $\mathcal{C}(\mathcal{X}; \sigma \circ g^m) \subseteq \mathcal{C}(\mathcal{X})$, it follows that

$$\mathcal{W}_{\epsilon, \tilde{\mathcal{Z}}}((\sigma \circ g^m)_{\#} \mathbb{P}_{\mathcal{X}}^i, (\sigma \circ g^m)_{\#} \mathbb{P}_{\mathcal{X}}^j) \leq \tilde{\mathcal{W}}_{\epsilon, \mathcal{X}}(\mathbb{P}^i, \mathbb{P}^j; \sigma \circ g^m). \quad (\text{B.4})$$

On the other hand, from the first order optimality condition and the continuity of $\sigma \circ g^m$, presented in Lemma 3.4, it follows that the optimal potentials $f^*, h^* \in \mathcal{C}(\mathcal{X})$, which realize the supremum in (B.3), are given by, respectively,

$$\begin{aligned}
f^*(x) &:= -\epsilon \log \left(\int_{\mathcal{X}} e^{\frac{1}{\epsilon}(h^*(y) - \|(\sigma \circ g^m)(x) - (\sigma \circ g^m)(y)\|^2)} d\mathbb{P}_{\mathcal{X}}^j(y) \right), \quad x \in \mathcal{X}, \\
h^*(y) &:= -\epsilon \log \left(\int_{\mathcal{X}} e^{\frac{1}{\epsilon}(f^*(x) - \|(\sigma \circ g^m)(x) - (\sigma \circ g^m)(y)\|^2)} d\mathbb{P}_{\mathcal{X}}^i(x) \right), \quad y \in \mathcal{X},
\end{aligned}$$

which can be represented by $f^* = \tilde{f}^* \circ \sigma \circ g^m$ and $h^* = \tilde{h}^* \circ \sigma \circ g^m$, respectively, where $\tilde{f}^*, \tilde{h}^* \in \mathcal{C}(\tilde{\mathcal{Z}})$ are given by, respectively,

$$\begin{aligned}
\tilde{f}^*(x) &:= -\epsilon \log \left(\int_{\mathcal{X}} e^{\frac{1}{\epsilon}(\tilde{h}^* \circ \sigma \circ g^m)(y) - \|x - (\sigma \circ g^m)(y)\|^2} d\mathbb{P}_{\mathcal{X}}^j(y) \right), \quad x \in \tilde{\mathcal{Z}}, \\
\tilde{h}^*(y) &:= -\epsilon \log \left(\int_{\mathcal{X}} e^{\frac{1}{\epsilon}(\tilde{f}^* \circ \sigma \circ g^m)(x) - \|(\sigma \circ g^m)(x) - y\|^2} d\mathbb{P}_{\mathcal{X}}^i(x) \right), \quad y \in \tilde{\mathcal{Z}}.
\end{aligned}$$

This ensures that $f^*, h^* \in \mathcal{C}(\mathcal{X}; \sigma \circ g^m) \subseteq \tilde{\mathcal{C}}(\mathcal{X})$. Hence we establish that (B.4) holds as equality.

From this and the Lipschitz continuity of $\sigma \circ g^m$ with the constant $C_{\sigma \circ g^m} > 0$ in Lemma 3.4, it follows that

$$\begin{aligned} \mathcal{W}_{\epsilon, \tilde{\mathcal{Z}}}((\sigma \circ g^m)_{\#} \mathbb{P}_{\mathcal{X}}^i, (\sigma \circ g^m)_{\#} \mathbb{P}_{\mathcal{X}}^j) &= \widetilde{\mathcal{W}}_{\epsilon, \mathcal{X}}(\mathbb{P}^i, \mathbb{P}^j; \sigma \circ g^m) \\ &\leq \inf_{\pi \in \Pi(\mathbb{P}^i, \mathbb{P}^j; \mathcal{X})} \left\{ \int_{\mathcal{X} \times \mathcal{X}} \left(C_{\sigma \circ g^m}^2 \|x - y\|^2 + \epsilon \log \left(\frac{d\pi(x, y)}{d\mathbb{P}_{\mathcal{X}}^i(x) d\mathbb{P}_{\mathcal{X}}^j(y)} \right) \right) d\pi(x, y) \right\} \\ &\leq \max\{C_{\sigma \circ g^m}^2, 1\} \mathcal{W}_{\epsilon, \mathcal{X}}(\mathbb{P}^i, \mathbb{P}^j). \end{aligned}$$

Therefore, we have shown that

$$\sum_{m=1}^M \max_{i, j \in \{1, \dots, K\}, i \neq j} \mathcal{W}_{\epsilon, \tilde{\mathcal{Z}}}((\sigma \circ g^m)_{\#} \mathbb{P}_{\mathcal{X}}^i, (\sigma \circ g^m)_{\#} \mathbb{P}_{\mathcal{X}}^j) \leq C \max_{i, j \in \{1, \dots, K\}, i \neq j} \mathcal{W}_{\epsilon, \mathcal{X}}(\mathbb{P}^i, \mathbb{P}^j),$$

with $C = \sum_{m=1}^M \max\{C_{\sigma \circ g^m}^2, 1\}$. Combining this with (B.1) concludes the proof. \square

C DETAILS ON EXPERIMENTS

C.1 EXPERIMENTAL ENVIRONMENT

We conduct all experiments using the specifications below:

- CPU: Intel(R) Xeon(R) Platinum 8163 CPU @ 2.50GHz.
- GPU: NVIDIA TITAN RTX.

All analyses in Section C.5 utilize the same environment. The comprehensive software setup can be found on GitHub.

C.2 DATASET CONFIGURATION

The training data generation follows the steps detailed below:

1. Retrieve financial data `{commodity, income, interest rate, exchange rate}` from the Federal Reserve Economic Data (FRED), and weather data `{pressure, rain, temperature, wind}` from the National Centers for Environmental Information (NCEI). Subsequently, we designate finance and weather as the superdomain \mathcal{A} , with the subordinate data categorized as individual domains.
2. Process each data point into a sliding window of defined dimensions $[\alpha, \beta]$, e.g., $[50, 10]$, with the sliding stride of 1. Each segment is treated as an individual instance.
3. To alleviate any potential concerns arising from data imbalance, we establish a predetermined quantity of 75,000 instances for each domain through random sampling, thereby guaranteeing independence from such considerations.
4. We randomly split each domain into three sets: 70% for training, 10% for validation, and 20% for testing.

It is worth noting that our dataset consists entirely of real-world data and covers a wide range of frequencies, including daily, weekly, monthly, quarterly, and yearly observations. The graphical representation of the frequency distribution for instances is depicted in Figure 3.

ODG scenarios involve no overlap between the source and target domains with respect to the superdomain, e.g., $\{\mathcal{D}\}_{k=1}^3 = \{\text{pressure, rain, temperature}\}$, and $\mathcal{D}^T = \text{commodity}$. For fair comparisons, the number of source domains is standardized to three across CDG and IDG scenarios. In CDG, we select one domain from the target domain's superdomain ($p = 2$) and two domains from the other superdomain as sources, e.g., $\{\mathcal{D}\}_{k=1}^3 = \{\text{commodity, income, pressure}\}$, and $\mathcal{D}^T = \text{rain}$. To evaluate IDG, we designate one target domain and consider the remaining domains within the same superdomain as source domains, e.g., $\{\mathcal{D}\}_{k=1}^3 = \{\text{pressure, rain, temperature}\}$, and $\mathcal{D}^T = \text{wind}$.

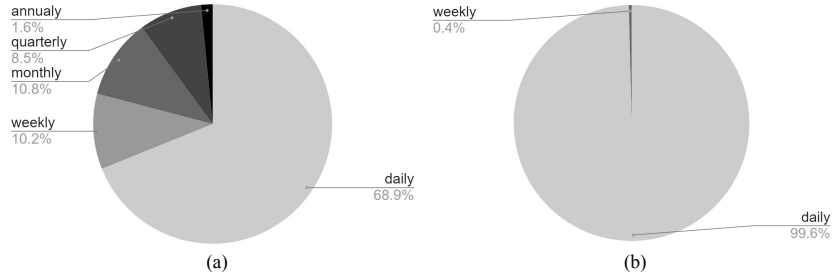


Figure 3: Visualization of frequency distribution. (a) FRED, and (b) NCEI.

Note that each selected combination of source domains for Table 2 is $\{\text{rain, temperature, wind}\}$ for ODG, $\{\text{commodity, temperature, wind}\}$ for CDG, and $\{\text{commodity, income, interest rate}\}$ for IDG.

C.3 EVALUATION METRICS

For our experiments, we employ two evaluation metrics. Given $H = N \times \beta$ with where N represents the number of instances, the metrics are defined as:

$$\text{sMAPE} = \frac{2}{H} \times \sum_{i=1}^H \frac{|y_i - \hat{y}_i|}{|y_i| + |\hat{y}_i|}, \quad \text{and} \quad \text{MASE} = \frac{1/H \times \sum_{i=1}^H |y_i - \hat{y}_i|}{1/(H-1) \times \sum_{i=1}^{H-1} |y_{i+1} - y_i|}.$$

C.4 HYPERPARAMETERS

Considering the scope of our experimental configuration that bring a total of 184 experimental cases for each model, we adopt a suitable range of hyperparameters to achieve the performance results presented in Table 1.

Table 3: Hyperparameters.

Hyperparameter	Considered Values
Lookback horizon.	$\alpha = 50$
Forecast horizon.	$\beta = 10$
Number of stacks.	$M = 3$
Number of blocks in each stack.	$L = 4$
Activation function.	ReLU
Feature dimension.	$\gamma = 512$
Loss function.	$\mathcal{L} = \text{sMAPE}$
Regularizing temperature.	$\lambda \in \{0.1, 0.3, 1, 3\}$
Learning rate scheduling.	CyclicLR(base_lr=2e-7, max_lr=2e-5, mode="triangular2", step_size_up=10)
Batch size.	$B = 2^{12}$
Number of iterations.	1,000
Type of stacks used for N-BEATS-I.	[Trend, Seasonality, Seasonality]
Number of polynomials and harmonics used for N-BEATS-I.	2
Pooling method used for N-HiTS.	MaxPool1d
Interpolation method used for N-HiTS.	interpolate(mode="linear")
Kernel size used for N-HiTS.	2

C.5 EXTENDED RESULTS

Tables 4 and 5 contain the extended experimental results summarized in Table 1. The suitability of various measures of dispersion within our proposed framework explored in Table 2 is presented in Tables 6 and 7 with more details. Specifically, we consider the commonly used metrics for the representation learning framework: for $\mu, \nu \in \mathcal{P}(\tilde{\mathcal{Z}})$,

- Kullback-Leibler divergence (KL):

$$\text{KL}(\mu\|\nu) = \int_{\tilde{\mathcal{Z}}} \log\left(\frac{\mu(dz)}{\nu(dz)}\right) \mu(dz),$$

- Maximum mean discrepancy (MMD):

$$\text{MMD}_{\mathcal{F}}(\mu, \nu) = \sup_{f \in \mathcal{F}} \left(\int_{\tilde{\mathcal{Z}}} f(x) \mu(dx) - \int_{\tilde{\mathcal{Z}}} f(y) \nu(dy) \right),$$

where \mathcal{F} represents a class of functions $f : \tilde{\mathcal{Z}} \rightarrow \mathbb{R}$. Notably, \mathcal{F} can be delineated as the unit ball in a reproducing kernel Hilbert space. For detailed description and insights into other possible function classes, refer to [22, Sections 2.2, 7.1, and 7.2].

Table 4: Evaluation of Feature-aligned N-BEATS. The first two columns denote the target domain for each experiment. This is followed in subsequent tables as well.

Methods		N-HITS		+ FA (Ours)		N-BEATS-I		+ FA (Ours)		N-BEATS-G		+ FA (Ours)	
Metrics		sMAPE	MASE	sMAPE	MASE	sMAPE	MASE	sMAPE	MASE	sMAPE	MASE	sMAPE	MASE
ODG													
FREI	Commodity	0.136	0.049	0.103	0.046	0.279	0.072	0.258	0.069	0.195	0.052	0.136	0.049
	Income	0.299	0.057	0.298	0.055	0.369	0.082	0.335	0.075	0.305	0.056	0.304	0.055
	Interest rate	0.120	0.074	0.100	0.070	0.200	0.044	0.189	0.046	0.148	0.073	0.120	0.073
	Exchange rate	0.035	0.059	0.034	0.058	0.078	0.078	0.075	0.069	0.040	0.062	0.039	0.060
	Average	0.148	0.060	0.134	0.057	0.232	0.069	0.214	0.065	0.172	0.061	0.150	0.059
NCEI	Pressure	0.368	0.255	0.350	0.250	0.759	0.396	0.409	0.305	0.368	0.255	0.367	0.255
	Rain	1.821	1.099	1.804	0.910	1.798	1.600	1.793	1.430	1.818	1.100	1.806	0.918
	Temperature	0.247	0.245	0.245	0.243	0.247	0.353	0.246	0.255	0.247	0.245	0.246	0.244
	Wind	0.455	0.645	0.454	0.644	0.451	0.665	0.449	0.662	0.455	0.645	0.454	0.645
	Average	0.723	0.561	0.713	0.512	0.814	0.754	0.724	0.663	0.722	0.561	0.718	0.516
CDG													
FREI	Commodity	0.082	0.047	0.081	0.044	0.195	0.060	0.197	0.059	0.119	0.046	0.107	0.046
	Income	0.296	0.054	0.295	0.053	0.327	0.072	0.323	0.070	0.301	0.055	0.295	0.053
	Interest rate	0.086	0.074	0.085	0.074	0.146	0.051	0.146	0.054	0.102	0.077	0.100	0.077
	Exchange rate	0.032	0.056	0.029	0.055	0.054	0.074	0.055	0.063	0.032	0.056	0.031	0.055
	Average	0.124	0.058	0.123	0.057	0.181	0.064	0.179	0.062	0.139	0.059	0.133	0.058
NCEI	Pressure	0.375	0.264	0.372	0.260	0.408	0.307	0.405	0.299	0.540	0.374	0.372	0.263
	Rain	1.807	1.169	1.803	0.783	1.800	2.091	1.787	1.831	1.807	1.169	1.804	1.178
	Temperature	0.334	0.243	0.245	0.242	0.275	0.245	0.240	0.244	0.253	0.245	0.245	0.243
	Wind	0.453	0.643	0.452	0.643	0.441	0.646	0.439	0.646	0.453	0.643	0.452	0.643
	Average	0.742	0.581	0.718	0.482	0.731	0.822	0.718	0.755	0.763	0.608	0.718	0.582
IDG													
FREI	Commodity	0.083	0.045	0.068	0.043	0.125	0.053	0.126	0.053	0.165	0.143	0.080	0.044
	Income	0.299	0.058	0.297	0.054	0.305	0.055	0.302	0.055	0.301	0.056	0.298	0.055
	Interest rate	0.072	0.081	0.071	0.081	0.088	0.084	0.086	0.091	0.080	0.083	0.074	0.081
	Exchange rate	0.024	0.051	0.024	0.050	0.028	0.056	0.029	0.056	0.025	0.051	0.024	0.050
	Average	0.119	0.059	0.115	0.057	0.137	0.062	0.136	0.064	0.143	0.083	0.119	0.058
NCEI	Pressure	0.394	0.276	0.384	0.272	0.392	0.266	0.389	0.263	0.384	0.276	0.384	0.276
	Rain	1.776	1.211	1.776	1.208	1.792	2.922	1.805	3.046	1.818	1.690	1.776	1.208
	Temperature	0.247	0.242	0.247	0.242	0.234	0.231	0.231	0.227	0.247	0.242	0.245	0.241
	Wind	0.455	0.641	0.452	0.640	0.433	0.622	0.434	0.623	0.454	0.641	0.452	0.640
	Average	0.718	0.593	0.715	0.591	0.713	1.011	0.715	1.039	0.726	0.712	0.714	0.591

Table 5: Comparison with competing models. Note that ‘NA’ indicates an anomalous error exceeding 10,000, not a divergence of training.

Methods		NLinear		DLinear		Autoformer		Informer	
Metrics		sMAPE	MASE	sMAPE	MASE	sMAPE	MASE	sMAPE	MASE
ODG									
FREI	Commodity	0.666	17.941	0.657	18.084	0.830	22.325	1.248	40.580
	Income	0.003	162.32	0.185	8,752.66	0.762	NA	1.275	NA
	Interest rate	0.022	9.138	0.190	83.204	0.363	144.97	1.209	2184.78
	Exchange rate	0.013	3.189	0.196	3.979	0.326	4.531	1.124	27.990
Average		0.176	48.147	0.307	2214.482	0.570	NA	1.214	NA
NCEI	Pressure	0.954	3.837	1.300	4.237	1.168	4.749	1.414	8.284
	Rain	1.038	1.089	1.231	1.169	1.175	0.897	1.783	1.162
	Temperature	1.136	4.399	1.340	4.572	1.352	5.761	1.616	10.885
	Wind	1.320	1.623	1.337	1.497	1.476	1.836	1.706	2.803
Average		1.112	2.737	1.302	2.869	1.293	3.311	1.630	5.784
CDG									
FREI	Commodity	0.664	18.166	0.855	21.661	0.829	21.360	1.353	40.584
	Income	0.004	212.60	0.203	9,979.14	0.995	NA	1.204	NA
	Interest rate	0.023	9.364	0.587	210.91	0.957	1,695.19	1.040	2,058.07
	Exchange rate	0.014	3.586	0.499	5.352	0.792	14.055	0.974	28.157
Average		0.176	60.929	0.536	2554.266	0.893	NA	1.098	NA
NCEI	Pressure	0.923	3.81	1.055	4.100	1.127	4.769	1.222	5.851
	Rain	1.037	1.137	1.033	1.125	1.201	0.899	1.523	1.149
	Temperature	1.114	4.340	1.106	4.431	1.304	5.609	1.439	7.358
	Wind	1.310	1.649	1.151	1.491	1.458	1.655	1.565	2.228
Average		1.096	2.734	1.086	2.787	1.273	3.233	1.437	4.147
IDG									
FREI	Commodity	0.671	30.210	1.139	38.929	0.835	21.462	1.652	34.784
	Income	0.026	1,951.16	0.043	4,232.97	1.500	NA	0.704	NA
	Interest rate	0.079	52.007	1.111	586.24	0.943	475.12	0.593	333.18
	Exchange rate	0.013	5.443	1.080	11.873	0.726	5.815	0.424	5.255
Average		0.197	509.705	0.843	1217.503	1.001	NA	0.843	NA
NCEI	Pressure	0.868	5.271	0.698	5.318	1.280	6.992	1.906	4.614
	Rain	0.900	1.368	0.709	1.301	1.009	0.918	1.463	1.081
	Temperature	1.014	6.055	0.768	5.753	1.310	4.788	1.080	4.235
	Wind	1.206	2.195	0.913	2.084	1.472	1.592	1.570	1.986
Average		0.997	3.722	0.772	3.614	1.268	3.573	1.530	2.979

Table 6: Comparison of divergences.

Models		N-HITS				N-BEATS-1				N-BEATS-G			
Divergences		KL		MMD		KL		MMD		KL		MMD	
Metrics		sMAPE	MASE	sMAPE	MASE	sMAPE	MASE	sMAPE	MASE	sMAPE	MASE	sMAPE	MASE
ODG													
FREI	Commodity	0.100	0.047	0.110	0.046	0.222	0.063	0.246	0.066	0.133	0.050	0.137	0.050
	Income	0.293	0.050	0.302	0.056	0.320	0.067	0.338	0.082	0.300	0.052	0.305	0.055
	Interest rate	0.100	0.070	0.107	0.083	0.189	0.046	0.165	0.021	0.120	0.073	0.123	0.077
	Exchange rate	0.040	0.053	0.034	0.058	0.070	0.070	0.074	0.073	0.044	0.057	0.041	0.059
Average		0.133	0.055	0.138	0.061	0.200	0.062	0.206	0.061	0.149	0.058	0.152	0.060
NCEI	Pressure	NaN	NaN	0.351	0.250	NaN	NaN	0.412	0.306	0.365	0.263	0.367	0.254
	Rain	NaN	NaN	1.820	0.919	NaN	NaN	1.800	1.728	1.831	0.951	1.818	1.026
	Temperature	NaN	NaN	0.246	0.244	NaN	NaN	0.248	0.255	0.248	0.247	0.248	0.245
	Wind	NaN	NaN	0.455	0.645	NaN	NaN	0.450	0.662	0.456	0.646	0.457	0.645
Average		NaN	NaN	0.718	0.515	NaN	NaN	0.728	0.738	0.725	0.527	0.723	0.543
CDG													
FREI	Commodity	NaN	NaN	0.086	0.045	NaN	NaN	0.187	0.057	NaN	NaN	0.104	0.046
	Income	NaN	NaN	0.298	0.054	0.315	0.064	0.323	0.071	0.296	0.051	0.301	0.055
	Interest rate	NaN	NaN	0.088	0.076	0.115	0.035	0.141	0.051	0.088	0.076	0.100	0.078
	Exchange rate	0.030	0.055	0.029	0.056	0.044	0.071	0.054	0.066	0.031	0.057	0.031	0.057
Average		NaN	NaN	0.125	0.058	NaN	NaN	0.176	0.061	NaN	NaN	0.134	0.059
NCEI	Pressure	NaN	NaN	0.377	0.262	NaN	NaN	0.405	0.316	NaN	NaN	0.370	0.262
	Rain	NaN	NaN	1.815	0.940	NaN	NaN	1.791	1.934	NaN	NaN	1.808	1.108
	Temperature	NaN	NaN	0.245	0.243	NaN	NaN	0.241	0.245	NaN	NaN	0.246	0.244
	Wind	NaN	NaN	0.453	0.643	NaN	NaN	0.440	0.646	NaN	NaN	0.453	0.643
Average		NaN	NaN	0.723	0.522	NaN	NaN	0.719	0.785	NaN	NaN	0.719	0.564
IDG													
FREI	Commodity	NaN	NaN	0.068	0.044	NaN	NaN	0.122	0.050	NaN	NaN	0.082	0.045
	Income	NaN	NaN	0.299	0.057	NaN	NaN	0.308	0.058	NaN	NaN	0.301	0.056
	Interest rate	NaN	NaN	0.072	0.080	NaN	NaN	0.098	0.089	NaN	NaN	0.074	0.082
	Exchange rate	NaN	NaN	0.025	0.051	NaN	NaN	0.035	0.055	0.026	0.049	0.025	0.051
Average		NaN	NaN	0.116	0.058	NaN	NaN	0.141	0.063	NaN	NaN	0.121	0.059
NCEI	Pressure	0.403	0.286	0.403	0.286	0.380	0.261	0.384	0.259	0.376	0.274	0.378	0.275
	Rain	NaN	NaN	1.849	1.421	NaN	NaN	1.792	2.881	NaN	NaN	1.817	1.687
	Temperature	NaN	NaN	0.247	0.242	NaN	NaN	0.234	0.228	NaN	NaN	0.245	0.242
	Wind	NaN	NaN	0.454	0.640	NaN	NaN	0.435	0.624	NaN	NaN	0.452	0.641
Average		NaN	NaN	0.738	0.647	NaN	NaN	0.711	0.998	NaN	NaN	0.723	0.711

Table 7: Comparison of ϵ values.

Models		N-HITS				N-BEATS-I				N-BEATS-G			
ϵ Values		1e-5		1e-1		1e-5		1e-1		1e-5		1e-1	
Metrics		sMAPE	MASE	sMAPE	MASE	sMAPE	MASE	sMAPE	MASE	sMAPE	MASE	sMAPE	MASE
ODG													
FRED	Commodity	0.103	0.046	0.109	0.047	0.257	0.069	0.121	0.097	0.11	0.047	0.112	0.074
	Income	0.297	0.055	0.297	0.129	0.334	0.075	0.329	0.267	0.302	0.057	0.304	0.204
	Interest rate	0.1	0.07	0.105	0.046	0.189	0.046	0.116	0.094	0.106	0.074	0.107	0.072
	Exchange rate	0.034	0.058	0.036	0.015	0.075	0.069	0.04	0.031	0.036	0.06	0.037	0.024
	Average	0.134	0.057	0.137	0.059	0.214	0.065	0.152	0.122	0.139	0.06	0.14	0.094
NCEI	Pressure	0.348	0.25	0.356	0.156	0.408	0.305	0.393	0.322	0.364	0.254	0.364	0.246
	Rain	1.795	0.91	1.79	0.776	1.789	1.43	1.98	1.603	1.808	0.944	1.832	1.223
	Temperature	0.244	0.243	0.246	0.106	0.245	0.255	0.272	0.219	0.247	0.244	0.252	0.167
	Wind	0.452	0.644	0.45	0.195	0.448	0.662	0.498	0.404	0.457	0.645	0.461	0.308
	Average	1.072	0.58	1.073	0.466	1.099	0.868	1.187	0.963	1.086	0.599	1.098	0.735
CDG													
FRED	Commodity	0.081	0.044	0.087	0.057	0.197	0.059	0.093	0.085	0.087	0.045	0.088	0.066
	Income	0.295	0.053	0.298	0.193	0.323	0.07	0.318	0.29	0.298	0.056	0.302	0.225
	Interest rate	0.085	0.074	0.09	0.058	0.146	0.054	0.096	0.086	0.09	0.078	0.091	0.067
	Exchange rate	0.029	0.055	0.03	0.02	0.055	0.063	0.032	0.03	0.03	0.057	0.03	0.023
	Average	0.123	0.057	0.126	0.082	0.18	0.062	0.135	0.123	0.126	0.059	0.128	0.095
NCEI	Pressure	0.372	0.26	0.369	0.24	0.405	0.299	0.393	0.361	0.367	0.261	0.374	0.28
	Rain	1.803	0.783	1.79	1.163	1.787	1.831	1.91	1.747	1.801	0.965	1.816	1.355
	Temperature	0.245	0.242	0.245	0.159	0.24	0.244	0.261	0.239	0.246	0.244	0.248	0.185
	Wind	0.452	0.643	0.451	0.293	0.439	0.646	0.481	0.44	0.454	0.643	0.457	0.341
	Average	1.088	0.522	1.08	0.702	1.096	1.065	1.152	1.054	1.084	0.613	1.095	0.818
IDG													
FRED	Commodity	0.068	0.043	0.07	0.056	0.126	0.053	0.071	0.092	0.07	0.044	0.07	0.055
	Income	0.297	0.054	0.304	0.24	0.302	0.055	0.308	0.397	0.299	0.058	0.303	0.238
	Interest rate	0.071	0.081	0.072	0.058	0.086	0.091	0.073	0.095	0.073	0.085	0.072	0.057
	Exchange rate	0.024	0.05	0.025	0.02	0.029	0.056	0.025	0.033	0.025	0.05	0.025	0.02
	Average	0.115	0.057	0.118	0.094	0.136	0.064	0.119	0.154	0.117	0.059	0.118	0.093
NCEI	Pressure	0.384	0.273	0.389	0.31	0.389	0.263	0.395	0.512	0.386	0.277	0.388	0.307
	Rain	1.776	1.212	1.785	1.422	1.805	3.046	1.811	2.348	1.781	1.326	1.781	1.409
	Temperature	0.247	0.243	0.247	0.196	0.231	0.227	0.25	0.323	0.246	0.241	0.246	0.194
	Wind	0.452	0.642	0.452	0.36	0.434	0.623	0.459	0.595	0.452	0.64	0.451	0.357
	Average	1.08	0.743	1.087	0.866	1.097	1.655	1.103	1.43	1.084	0.802	1.085	0.858

D VISUAL EXPLORATION

In this section, we juxtapose the vanilla baseline models, i.e., N-BEATS-G, N-BEATS-I, and N-HITS, against our counterparts, gauging their forecasting quality through visual inspection. As illustrated in Figure 4, incorporating feature alignment remarkably bolsters generalizability, allowing the models to produce finer forecast details. Notably, while baseline models suffer significant accuracy degradation in the ODG and CDG scenarios, Feature-aligned N-BEATS evidences the benefits of the feature alignment.

To further investigate the representational landscape, we analyze the samples of push-forward measure from N-BEATS-I and N-HITS. Adopting visualization techniques for both aligned and non-aligned instances as depicted in Figure 1, we configure UMAP with 5 neighbors, a minimum distance of 0.1, and employ the Euclidean metric. Similar to N-BEATS-G, we discern two observations in Figure 5 pertaining to N-BEATS-I and N-HITS: (1) instances coalesce, residing closer to one another, and (2) an evident surge in domain entropy, from both N-BEATS-I and N-HITS.

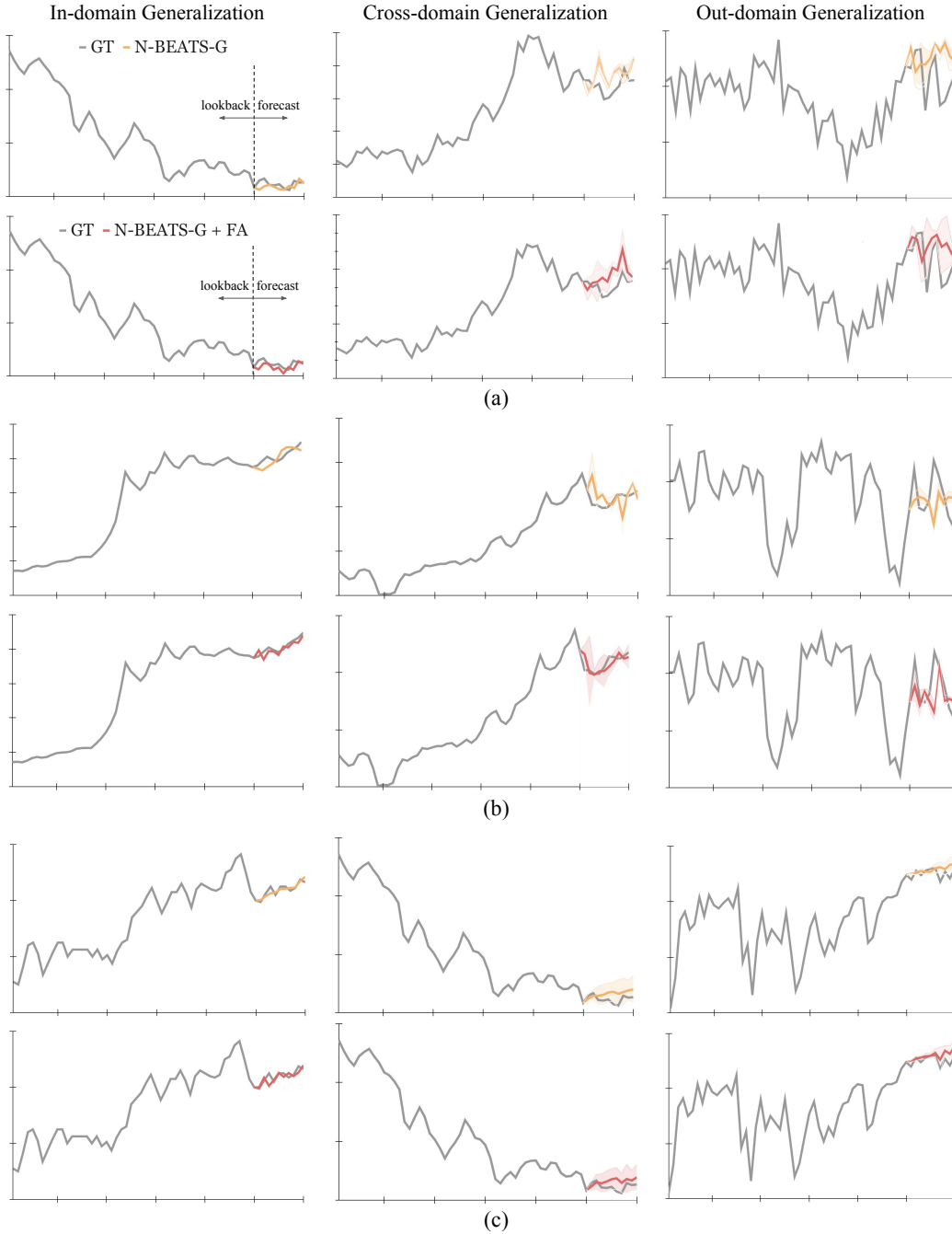


Figure 4: Visual comparison of forecasts. (a) N-BEATS-G, (b) N-BEATS-I, and (c) N-HITS. Results are averaged across source domain combinations, with standard deviations.

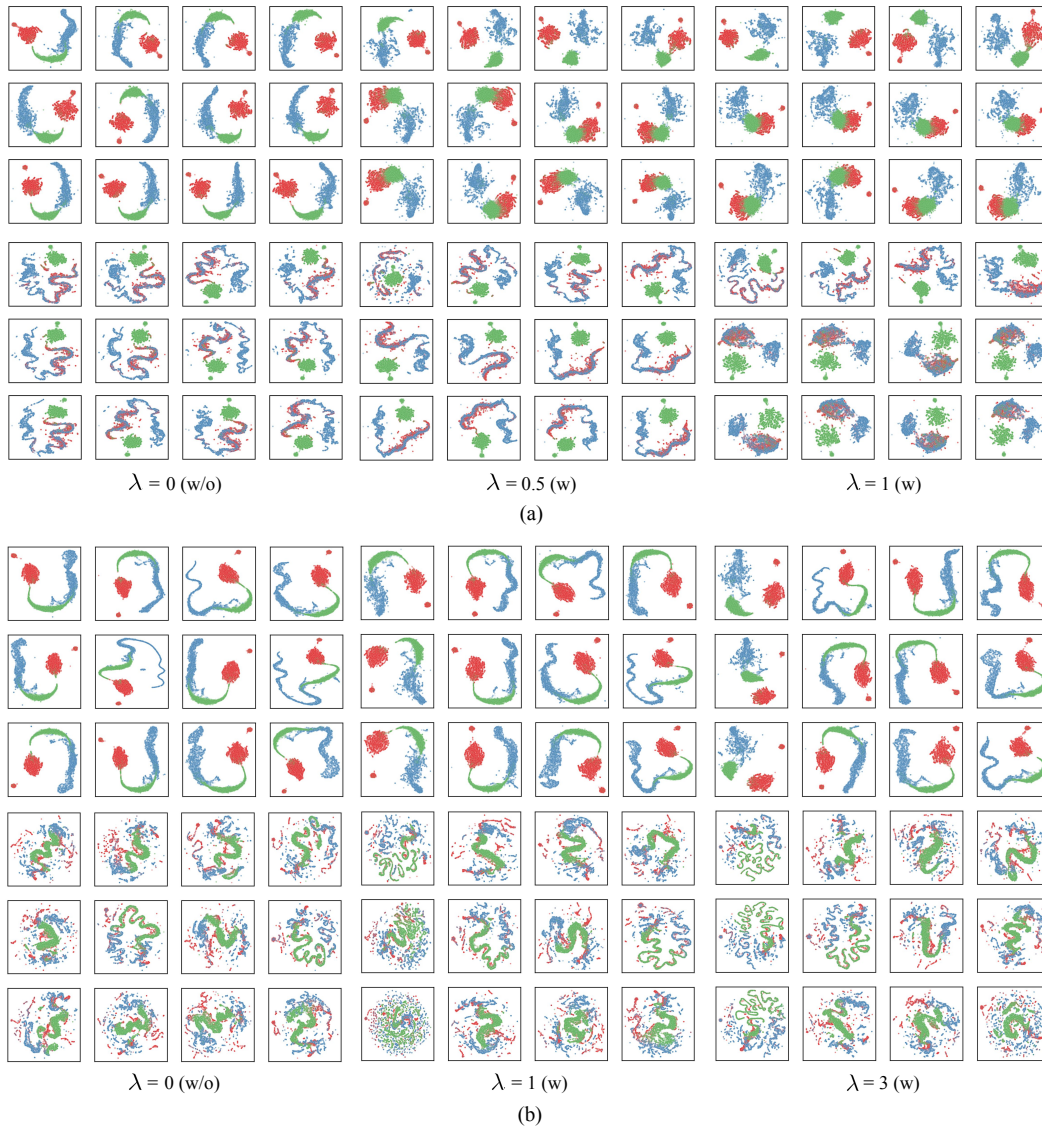


Figure 5: Visualization of extracted features. (a) N-BEATS-I, and (b) N-HiTS. For both (a) and (b), former plots illustrate increased inter-instance proximity, while subsequent ones depict inflated entropy.

E ABLATION STUDIES

E.1 ALIGNMENT FREQUENCIES

As mentioned in Remark 3.3, redundant gradient flows from recurrent architecture potentially causes gradient explosion or vanishing. To empirically validate this insight applied to our approach, we contrast stack-wise and block-wise feature alignments, as shown in Table 8. Notably, although stack-wise alignment generally outperform its counterpart, we do not observe the aforementioned problems, which could be identified by divergence of training. N-BEATS-I with block-wise alignment even demonstrates superior performance. Two plausible explanations are: (1) the limited number of stacks, and (2) the operational differences between the trend and seasonality modules in N-BEATS-I, which might help alleviating redundancy issue. Nonetheless, our primary objective of generalizing the recurrent model across various domains appears achievable through stack-wise alignment.

Table 8: Comparison between stack-wise and block-wise alignments.

Models		N-HITS				N-BEATS-I				N-BEATS-G			
		Block-wise		Stack-wise (Ours)		Block-wise		Stack-wise (Ours)		Block-wise		Stack-wise (Ours)	
Metrics		sMAPE	MASE	sMAPE	MASE	sMAPE	MASE	sMAPE	MASE	sMAPE	MASE	sMAPE	MASE
ODG													
FRED	Commodity	0.137	0.049	0.103	0.046	0.133	0.049	0.258	0.069	0.137	0.049	0.136	0.049
	Income	0.306	0.056	0.298	0.055	0.305	0.055	0.335	0.075	0.306	0.056	0.304	0.055
	Interest rate	0.121	0.074	0.1	0.07	0.119	0.073	0.189	0.046	0.121	0.075	0.12	0.073
	Exchange rate	0.04	0.06	0.034	0.058	0.04	0.06	0.075	0.069	0.04	0.06	0.039	0.06
	Average	0.122	0.122	0.122	0.122	0.149	0.059	0.214	0.065	0.151	0.06	0.15	0.059
NCEI	Pressure	0.368	0.255	0.35	0.25	0.367	0.254	0.409	0.305	0.368	0.255	0.367	0.255
	Rain	1.806	1.094	1.804	0.91	1.806	1.094	1.793	1.43	1.807	1.091	1.806	0.918
	Temperature	0.247	0.245	0.245	0.243	0.247	0.245	0.246	0.255	0.247	0.245	0.246	0.244
	Wind	0.456	0.645	0.454	0.644	0.456	0.645	0.449	0.662	0.457	0.645	0.454	0.645
	Average	0.122	0.122	0.122	0.122	1.087	0.674	1.101	0.868	1.088	0.673	1.087	0.587
CDG													
FRED	Commodity	0.102	0.046	0.081	0.044	0.105	0.046	0.197	0.059	0.108	0.047	0.107	0.046
	Income	0.301	0.054	0.295	0.053	0.301	0.055	0.323	0.07	0.301	0.054	0.295	0.053
	Interest rate	0.099	0.076	0.085	0.074	0.097	0.076	0.146	0.054	0.101	0.078	0.1	0.077
	Exchange rate	0.031	0.056	0.029	0.055	0.031	0.098	0.055	0.063	0.032	0.055	0.031	0.055
	Average	0.122	0.122	0.122	0.122	0.134	0.069	0.18	0.062	0.136	0.059	0.133	0.058
NCEI	Pressure	0.371	0.263	0.372	0.26	0.37	0.262	0.405	0.299	0.373	0.264	0.372	0.263
	Rain	1.809	1.144	1.803	0.783	1.808	1.148	1.787	1.831	1.804	1.181	1.804	1.178
	Temperature	0.246	0.244	0.245	0.242	0.246	0.244	0.24	0.244	0.246	0.244	0.245	0.243
	Wind	0.453	0.644	0.452	0.643	0.454	0.644	0.439	0.646	0.453	0.643	0.452	0.643
	Average	0.122	0.122	0.122	0.122	1.089	0.705	1.096	1.065	1.089	0.723	1.088	0.721
IDG													
FRED	Commodity	0.081	0.045	0.068	0.043	0.075	0.044	0.126	0.053	0.074	0.044	0.08	0.044
	Income	0.302	0.056	0.297	0.054	0.301	0.056	0.302	0.055	0.302	0.056	0.298	0.055
	Interest rate	0.079	0.083	0.071	0.081	0.079	0.082	0.086	0.091	0.079	0.083	0.074	0.081
	Exchange rate	0.025	0.051	0.024	0.05	0.025	0.051	0.029	0.056	0.025	0.051	0.024	0.05
	Average	0.122	0.122	0.122	0.122	0.12	0.058	0.136	0.064	0.12	0.059	0.119	0.058
NCEI	Pressure	0.384	0.276	0.384	0.272	0.383	0.277	0.389	0.263	0.384	0.276	0.384	0.276
	Rain	1.818	1.681	1.776	1.208	1.798	1.535	1.805	3.046	1.817	1.676	1.776	1.208
	Temperature	0.247	0.243	0.247	0.242	0.245	0.242	0.231	0.227	0.246	0.243	0.245	0.241
	Wind	0.453	0.641	0.452	0.64	0.453	0.641	0.434	0.623	0.453	0.641	0.452	0.64
	Average	0.122	0.122	0.122	0.122	1.091	0.906	1.097	1.655	1.101	0.976	1.08	0.742

E.2 NORMALIZING FUNCTIONS

According to the Table 9, Feature-aligned N-BEATS generally achieves superior performance when utilizing softmax function. However, there are instances where tanh function or even the absence of a normalization yields better results compared to the softmax. This suggests that while scale is predominant instance-wise attribute, it may exhibit domain-dependent characteristics under certain conditions. Aligning this scale is therefore necessary. This entails that the softmax, tanh, and to not normalize offer different levels of flexibility in modulating or completely disregarding the scale information, implying a spectrum of capacities in aligning domain-specific attributes.

E.3 SUBTLE DOMAIN SHIFT

Although the domain generalization commonly focuses on the domain shift problems, models may not perform as expected when the domain shift between source and target data is minimal. In some cases where the data from both domains align closely, fitting to source domain without invariant feature learning even can be beneficial. To examine this concern, we extend our analysis to the generalizability of Feature-aligned N-BEATS under such conditions. Table 10 demonstrates, while our model remains competitive, there is performance degradation observed in certain instances.

Table 9: Comparison of normalizing functions.

Models		N-HITS				N-BEATS-I				N-BEATS-G									
Normalizers		None		tanh		softmax (Ours)		None		tanh		softmax (Ours)							
Metrics		sMAPE	MASE	sMAPE	MASE	sMAPE	MASE	sMAPE	MASE	sMAPE	MASE	sMAPE	MASE						
ODG																			
FRED	Commodity	0.103	0.046	0.104	0.046	0.103	0.046	0.265	0.07	0.27	0.069	0.258	0.069	0.05	0.136	0.05	0.135	0.049	0.14
	Income	0.299	0.056	0.299	0.056	0.298	0.055	0.319	0.06	0.324	0.063	0.335	0.075	0.306	0.056	0.305	0.056	0.304	0.055
	Interest rate	0.101	0.071	0.101	0.071	0.1	0.07	0.191	0.073	0.193	0.048	0.189	0.046	0.12	0.072	0.123	0.074	0.12	0.073
	Exchange rate	0.034	0.058	0.034	0.058	0.034	0.058	0.072	0.061	0.077	0.074	0.075	0.069	0.041	0.061	0.043	0.059	0.039	0.06
	Average	0.134	0.058	0.135	0.058	0.134	0.057	0.212	0.066	0.216	0.064	0.214	0.065	0.129	0.081	0.13	0.081	0.128	0.082
NCEI	Pressure	0.349	0.25	0.348	0.249	0.35	0.25	0.398	0.289	0.411	0.3	0.409	0.305	0.352	0.247	0.361	0.253	0.367	0.255
	Rain	1.819	0.918	1.82	0.917	1.804	0.91	1.808	2.087	1.807	1.841	1.793	1.43	1.814	1.075	1.814	1.071	1.806	0.918
	Temperature	0.247	0.244	0.246	0.244	0.245	0.243	0.248	0.253	0.249	0.256	0.246	0.255	0.247	0.245	0.248	0.245	0.246	0.244
	Wind	0.455	0.645	0.455	0.644	0.454	0.644	0.452	0.66	0.451	0.661	0.449	0.662	0.456	0.645	0.457	0.645	0.454	0.645
	Average	1.084	0.584	1.084	0.583	1.077	0.58	1.103	1.188	1.109	1.071	1.101	0.868	1.083	0.661	1.088	0.662	1.087	0.587
CDG																			
FRED	Commodity	0.082	0.045	0.081	0.044	0.081	0.044	0.189	0.059	0.203	0.061	0.197	0.059	0.108	0.047	0.109	0.047	0.107	0.046
	Income	0.296	0.055	0.296	0.055	0.295	0.053	0.323	0.088	0.319	0.064	0.323	0.07	0.302	0.054	0.301	0.054	0.295	0.053
	Interest rate	0.085	0.074	0.085	0.075	0.085	0.074	0.145	0.052	0.149	0.058	0.146	0.054	0.101	0.078	0.101	0.077	0.1	0.077
	Exchange rate	0.029	0.056	0.029	0.056	0.029	0.055	0.053	0.066	0.055	0.065	0.055	0.063	0.032	0.056	0.032	0.056	0.031	0.055
	Average	0.123	0.058	0.123	0.058	0.123	0.057	0.178	0.066	0.182	0.062	0.18	0.062	0.136	0.059	0.136	0.059	0.133	0.058
NCEI	Pressure	0.373	0.26	0.374	0.26	0.372	0.26	0.405	0.316	0.41	0.313	0.405	0.299	0.255	0.372	0.257	0.356	0.263	0.355
	Rain	1.808	0.931	1.808	0.931	1.803	0.783	1.802	2.152	1.802	2.144	1.787	1.831	1.805	1.18	1.805	1.186	1.804	1.178
	Temperature	0.246	0.243	0.246	0.243	0.245	0.242	0.242	0.246	0.244	0.248	0.24	0.244	0.245	0.243	0.246	0.243	0.245	0.243
	Wind	0.453	0.643	0.453	0.643	0.452	0.643	0.442	0.649	0.443	0.649	0.439	0.646	0.643	0.452	0.643	0.453	0.643	0.453
	Average	1.091	0.596	1.091	0.596	1.088	0.522	1.104	1.234	1.106	1.229	1.096	1.065	1.03	0.776	1.031	0.771	1.034	0.767
IDG																			
FRED	Commodity	0.068	0.044	0.068	0.044	0.068	0.043	0.124	0.052	0.142	0.055	0.126	0.053	0.083	0.045	0.083	0.045	0.08	0.044
	Income	0.299	0.057	0.299	0.058	0.297	0.054	0.31	0.059	0.308	0.058	0.302	0.055	0.302	0.056	0.302	0.057	0.298	0.055
	Interest rate	0.072	0.081	0.072	0.077	0.071	0.081	0.097	0.087	0.104	0.079	0.086	0.091	0.08	0.081	0.08	0.08	0.074	0.081
	Exchange rate	0.025	0.051	0.025	0.05	0.024	0.05	0.033	0.055	0.04	0.055	0.029	0.056	0.026	0.052	0.026	0.051	0.024	0.05
	Average	0.116	0.058	0.116	0.057	0.115	0.057	0.141	0.063	0.149	0.062	0.136	0.064	0.123	0.059	0.123	0.058	0.119	0.058
NCEI	Pressure	0.393	0.273	0.393	0.273	0.384	0.272	0.373	0.256	0.39	0.266	0.389	0.263	0.366	0.274	0.367	0.283	0.384	0.276
	Rain	1.776	1.211	1.776	1.205	1.776	1.208	1.883	3.222	1.873	3.848	1.805	3.046	1.818	1.671	1.818	1.695	1.776	1.208
	Temperature	0.247	0.242	0.247	0.242	0.247	0.242	0.236	0.232	0.235	0.231	0.231	0.227	0.246	0.241	0.246	0.242	0.245	0.241
	Wind	0.454	0.641	0.454	0.64	0.452	0.64	0.441	0.631	0.441	0.632	0.434	0.623	0.453	0.642	0.452	0.642	0.452	0.64
	Average	1.085	0.742	1.085	0.739	1.08	0.74	1.128	1.739	1.132	2.057	1.097	1.655	1.092	0.973	1.093	0.989	1.08	0.742

Table 10: Evaluation under subtle domain shift. ‘F’ and ‘N’ represent the FRED and NCEI datasets, respectively. The number of domains associated with each dataset is denoted accordingly, e.g., ‘F3’ represents three source domains from FRED. We conduct experiments by considering all possible combinations for each case.

Methods	N-HITS		+ FA (Ours)		N-BEATS-I		+ FA (Ours)		N-BEATS-G		+ FA (Ours)	
	sMAPE	MASE	sMAPE	MASE	sMAPE	MASE	sMAPE	MASE	sMAPE	MASE	sMAPE	MASE
F3	0.023	2.055	0.023	2.055	0.025	2.028	0.027	2.061	0.024	2.064	0.024	2.066
F2N1	0.236	0.244	0.236	0.240	0.210	0.221	0.209	0.220	0.236	0.241	0.236	0.244
F1N2	0.235	0.240	0.235	0.240	0.209	0.220	0.209	0.219	0.235	0.240	0.234	0.241
N3	0.243	0.243	0.243	0.243	0.220	0.224	0.221	0.225	0.242	0.243	0.241	0.242
Average	0.184	0.695	0.184	0.694	0.166	0.673	0.166	0.680	0.184	0.697	0.184	0.698